European Transport Studies 1 (2024) 100002

Contents lists available at ScienceDirect

European Transport Studies

journal homepage: www.sciencedirect.com/journal/european-transport-studies

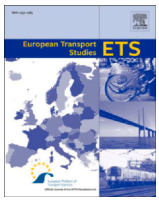

# Retrofitting of ultralight aircraft with a fuel cell power system

Teresa Donateo[a,*], Antonio Ficarella[a], Leonardo Lecce[b]

[a] Department of Engineering for Innovation, University of Salento, via per Monteroni, 73100 Lecce, Italy
[b] Novotech – Advanced Aerospace Technology, Srl, Naples, Italy

ARTICLE INFO

*Keywords:*
Hydrogen propulsion
Aircraft electrification
PEM fuel cell
Lithium batteries

ABSTRACT

Hydrogen power systems are one of the main development prospects of our century in all means of transportation. Among them, the conversion of hydrogen energy in a fuel cell system guarantees the highest value of efficiency. However, fuel cells need to be coupled with a secondary electric storage system in mobility applications because of their limitations in terms of dynamic response and power density. In the present investigation, the preliminary design of a hybrid electric power system with fuel cells for an ultralight aerial vehicle is addressed with a retrofitting approach. The proposed power system includes a fuel cell, a lithium battery, and a compressed hydrogen vessel to replace the conventional piston-prop configuration while keeping the same maximum take-off mass. A simple but comprehensive procedure is used to find the size of the power system components that minimize the total mass and satisfy the target of a size below 200 L. The inputs of the parametric analysis are the hybridization ratio and the type of lithium battery. The results of the analysis revealed that fuel cell systems are suitable for the electrification of ultralight aviation if the desired endurance is higher than 30 min In this case, batteries by high power density are needed to satisfy the power requirements at take-off. For shorter flight times, a battery configuration is to be preferred and energy density is the most critical parameters for the choice of the battery. The possibility of charging the battery on-board determines a larger fuel cell and a higher consumption of hydrogen than a charge depleting strategy (+10 %) but avoid long charging times between two consecutive flights.

## 1. Introduction

The need for forms of transportation, which are faster, cheaper, safer, and cleaner than today is more and more critical (Papadopoulos et al., 2018; ANON, 2023a). In fact, road travel is responsible for three-quarters of global carbon dioxide ($CO_2$) emissions (ec.europa.eu) while aviation accounts for 11.6 % of the total transport emission.

The use of hydrogen in fuel cells has the potential to achieve zero-emission transportation systems but requires innovation, research, and investment (Sparano et al., 2023). Today, the highest-efficiency solution for using hydrogen is represented by the Proton Exchange Membrane fuel cell (PEMFC) (Ayar and Karakoc, 2023). However, batteries or other electric storage systems must be coupled with the fuel cell in hybrid electric architectures to overcome the limitations of hydrogen systems (Geliev et al., 2019; Jarry et al., 2021a). A compressed or liquified hydrogen vessel has higher gravimetric energy density but lower volumetric energy density than lithium batteries while the fuel cell has a low power density compared with the battery (Thomas, 2009). The role of the battery in a fuel cell system is also to overcome the slower dynamic response of the fuel cell (Geliev et al., 2019). Hybridization, on the other hand, requires efficient energy management strategies and a careful consideration of operating conditions and technological limits (Lü et al., 2020; Park et al., 2022a). Fuel cell systems are often considered as energy sources and compared to batteries in terms of energy density (see for example (Geliev et al., 2019) where a 750 Wh/kg density is reported for a fuel cell). However, this is not correct because, differently from batteries, power and energy in a fuel cell system are decoupled (Beyers et al., 2023). The fuel cell is responsible only for power conversion while the energy content depends on the hydrogen storage system.

The mass of the fuel cell system affects the takeoff weight of the aircraft, which in turn affects its performance and flight duration (Geliev et al., 2019). Therefore, an accurate choice of its size is very important and some studies propose an optimization of the fuel cell system using as a metric the hydrogen fuel consumption and the total mass (Jarry et al., 2021a, 2021b). However, as pointed out by Nicolay et al (Nicolay et al., 2021)., the volumetric energy density is of equal

* Corresponding author.
*E-mail address:* teresa.donateo@unisalento.it (T. Donateo).

https://doi.org/10.1016/j.ets.2024.100002
Received 20 February 2024; Received in revised form 6 May 2024; Accepted 4 June 2024
Available online xxxx

**Nomenclature**

| | |
|---|---|
| $a$ | Acceleration. |
| $C_{nom,in}$ | Tentative value of battery nominal capacity |
| $C_{rate,ch}$ | Maximum battery rate of charge |
| $C_{rate,dis}$ | Maximum battery rate of discharge |
| $c_D$ | Drag coefficient |
| $c_L$ | Lift coefficient |
| $C_{nom}$ | Nominal capacity of the battery pack |
| $C_p$ | Propeller power coefficient |
| $C_T$ | Propeller thrust coefficient |
| $D$ | Drag force |
| $D_p$ | Propeller diameter |
| $E_{batt,nom,in}$ | Tentative value of battery nominal energy |
| $E_{batt}$ | Nominal energy of the battery |
| $E_{batt}(i)$ | Battery energy at flight phase $i$ |
| $E_{fuel}$ | Energy stored in the fuel tanks |
| $g$ | Gravity acceleration |
| $GED_{batt}$ | Gravimetric energy density of the battery |
| $GPD_{FC}$ | Gravimetric power density of the fuel cell |
| $H_2FR$ | Flow rate of hydrogen |
| $h_L$ | Flight altitude |
| $h_{\max}$ | Maximum flight altitude of the mission |
| $H_P$ | Power hybridization degree |
| $HHV_{H_2}$ | Heating value of hydrogen |
| $i$ | Flight phase (1,2,.,6) |
| $I_{\max,batt}$ | Maximum battery power during the mission |
| $I_{\max,ch}$ | Maximum battery current in charge |
| $I_{\max,dis}$ | Maximum battery current in discharge |
| $I_{\min,batt}(i)$ | Minimum battery power during the mission |
| $I_{st}$ | Stack current |
| $ID_b$ | Battery Identifier |
| $J$ | Propeller advance ratio |
| $L$ | Lift force |
| $M_{H_2tank}$ | Hydrogen vessel mass |
| $M_{batt}$ | Battery mass |
| $M_{FC}$ | Fuel cell mass. |
| $M_{H_2}$ | Mass of hydrogen consumed in the mission |
| $M_{tot}$ | Total mass of the propulsive system |
| $n$ | Propeller speed |
| $P$ | power |
| $P_{batt,nom}$ | Nominal power of the battery |
| $P_{EM,nom}$ | Nominal power of the electric machine |
| $P_{FC,nom}$ | Nominal power of the fuel cell |
| $P_{ICE,nom}$ | Nominal power of the engine |
| $P_{\max,ch}$ | Maximum battery power in charge |
| $P_{\max,dis}$ | Maximum battery power in discharge |
| $p_0$ | Atmospheric pressure at sea level |
| $P_{aux}$ | Power of aircraft auxiliary services |
| $P_{batt}(i)$ | Battery power at flight phase $i$ |
| $P_C$ | Propulsive power at climb |
| $P_{el}$ | Electric power |
| $P_{FC}(i)$ | Fuel cell power at flight phase $i$ |
| $P_{net}$ | Net power of the fuel cell |
| $P_{par}$ | Parasitic power of the Balance of Plant |
| $P_{takeoff}$ | Electric power required by the electric motor during take-off |
| $P_{TOT}$ | Total installed power |
| $RC$ | Rate of climb |
| $\rho$ | Density |
| S | Wing area |
| $T$ | Thrust |
| $t$ | Time |
| $T_0$ | Atmospheric temperature at sea level |
| $T_C$ | Required thrust to counterbalance the gravitational force |
| $T_{climb}$ | Thrust at climb |
| $t_{\min}$ | Total flight time in minutes |
| $V$ | Aircraft true air speed |
| $V_{H_2tank}$ | Hydrogen vessel volume |
| $V_{batt}$ | Nominal voltage of the battery pack |
| $V_{batt}$ | Battery volume |
| $V_{FC}$ | Fuel cell volume |
| $V_{lo}$ | Lift-off speed |
| $V_{st}$ | Stack voltage |
| $V_{tot}$ | Total volume of the propulsive system |
| $VED_{H_2}$ | Volumetric energy density of compressed hydrogen at 700 bar |
| $VED_{H_2}$ | Volumetric energy density of hydrogen storage system |
| $VED_{batt}$ | Volumetric energy density of the battery |
| $VPD_{FC}$ | Volumetric gravity density of the fuel cell |
| $W$ | Aircraft weight |
| $W_{TO}$ | Take-off weight |
| $x_{FC}$ | Fuel cell contribution to the take-off power |
| $\Delta E_{batt}$ | Range of variation of battery energy during the mission |
| $\Delta t(i)$ | Time duration of flight phase $i$ |
| $\eta_{EM}$ | Efficiency of the electric machine |
| $\eta_{FC}$ | Net efficiency of the fuel cell |
| $\eta_P$ | Propeller efficiency |
| $\eta_{stor}$ | Storing efficiency |
| $\eta_T$ | Gearbox efficiency |
| $\eta_{DC-DC}$ | Efficiency of the DC-DC converter |

*List of acronyms*

| | |
|---|---|
| BOP | Balance of the Plant |
| CD | Charge Depleting |
| CS | Charge Sustaining |
| DOD | Depth of Discharge of the battery |
| EMS | Energy management strategy |
| GED | Gravimetric energy density |
| HEX | Heat Exchanger |
| HT-PEM | High-temperature proton exchange membrane fuel cell |
| ISA | International Standard Atmosphere |
| LCO | $LiCoO_2$ – Graphite battery |
| LFP | $LiFePO_4$ – Graphite battery |
| Li-po | Lithium-polymer battery |
| LMO | (LiMn2O4 – Graphite battery |
| LTO | Various - $Li_4Ti_{15}O_{12}$ battery |
| MEA | membrane electrolyte assembly |
| NCA | $LiNiCoAlO_2$ – Graphite battery |
| NMC | $LiNiMnCoO_2$ – Graphite battery |
| PEMFC | Proton Exchange Membrane Fuel Cell |
| SOC | State of charge of the battery |
| UAV | Unmanned Aerial Vehicle |
| VED | Volumetric energy density |

importance in the aerospace field (Ayar and Karakoc, 2023), particularly in a small vehicle.

One of the difficulties in developing a comprehensive sizing methodology is the multi-physic nature of hybrid electric power systems with fuel cells (Geliev et al., 2019) that makes necessary to take into account the technological limits of each component. Otherwise, the validity of the sizing procedure can be questioned like in (Park et al., 2022a) and (Park et al., 2022b).

The present investigation proposes a parametric analysis for the sizing of the three main components of a hydrogen hybrid electric

architecture: the fuel cell, the battery, and the hydrogen vessel. The procedure is applied to the preliminary design of a small-scale hydrogen demonstrator for ultralight aviation that will be assembled and tested in the framework of a research project named SERENA. To this scope, a constant takeoff weight is assumed in the investigation. However, with expected technological improvements, the maximum takeoff weight (MTOM) of a fuel cell aircraft could potentially be lower than that of a conventional aircraft (Marksel and Prapotnik Brdnik, 2022) in the future.

The manuscript is organized as follows. Section 2 presents the background and motivations for this work and highlights the novelty of the proposed approach. Section 3 introduces the specification of the ultralight aircraft together with the choice of reference missions and the details of the propeller and the electric machines. The sizing methodology is described in Section 4, where the technological specifications of fuel cells, batteries, and hydrogen storage systems adopted in the investigation are also discussed. Section 5 analyzes the results of the methodology in terms of battery technology, charging choice for the battery, and mission specification. These results are used to select the final configuration and discuss economic and environmental issues in Section 6. Some future studies needed to overcome the limitation of the methodology are proposed in Section 7. Section 8 summarizes and generalizes the results of the investigation.

## 2. Background and motivations

The present investigation is aimed at reducing the environmental impact for a ultralight aerial vehicle. For this class of vehicles, gasoline piston engines are generally used (Wróblewski, 2022) but hybrid electric configurations with piston engines (Wróblewski et al., 2023; Pisapia et al., 2023) or PEMFC fuel cells have been also proposed (Geliev et al., 2019). The heart of a PEMFC cell is the membrane electrolyte assembly (MEA) enclosed between gas diffusion layers and the cathode and anode flow channels (see Fig. 1). Since the average voltage of a single cell is quite low (0.6 – 0.7 V), a certain number of cells are connected in series to reach the desired voltage, obtaining a stack. The stack needs to be integrated with other components for the management of reactants, water, heat, and electricity. Such sub-systems form the so-called Balance of the Plant (BOP).

Based on the type of air management, fuel cell systems can be classified into open-cathode and closed-cathode (Xing et al., 2022). In an open-cathode configuration, a fan is used to deliver a mass flow rate of air that has the double task of delivering oxygen to the stack and removing the heat generated by the chemical reactions. Air-cooled open-cathode fuel cell systems are adopted in the range of 0.1–6 kW. For higher values, the heat released from the electrochemical reaction may not be sufficiently removed without a separate cooling circuit. Moreover, the reactant supplied to the cell may not be sufficient to sustain the optimum electrochemical reaction, especially at high altitudes.

A closed-cathode configuration allows accurate control of the airflow rate at high altitudes thanks to the separation between the (liquid) cooling system and the cathode air circuit. This is obtained, however, at the expense of a more complex balance of plants. A typical configuration of a closed-cathode fuel cell system for aerospace applications is represented in Fig. 2. Note the presence of three interconnected subsystems (hydrogen supply, air delivery, and temperature regulation), the need for a radiator as a heat exchanger (HEX), and the presence of a DC/DC converter to adapt the voltage of the stack to the load. Additionally, a water management circuit may be necessary if the stack is not self-humidified. The hydrogen is taken from the tank through a regulation valve and sent to the anode which usually presents a dead-end configuration with a purge valve for the elimination of water and impurities. Hydrogen recirculation is also possible. The air is

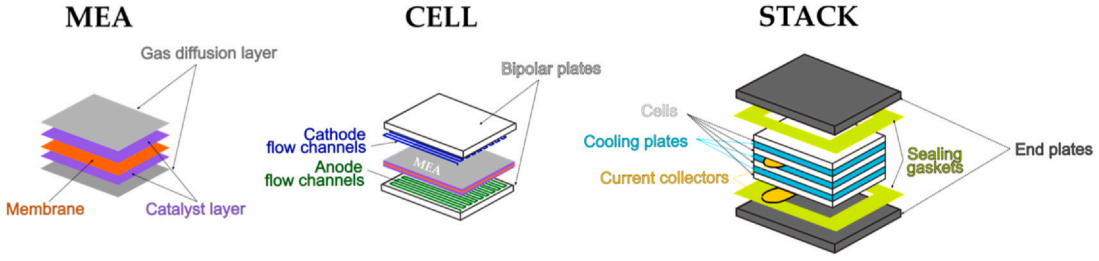


**Fig. 1.** Structure of a PEMFC (Donateo, 2023).

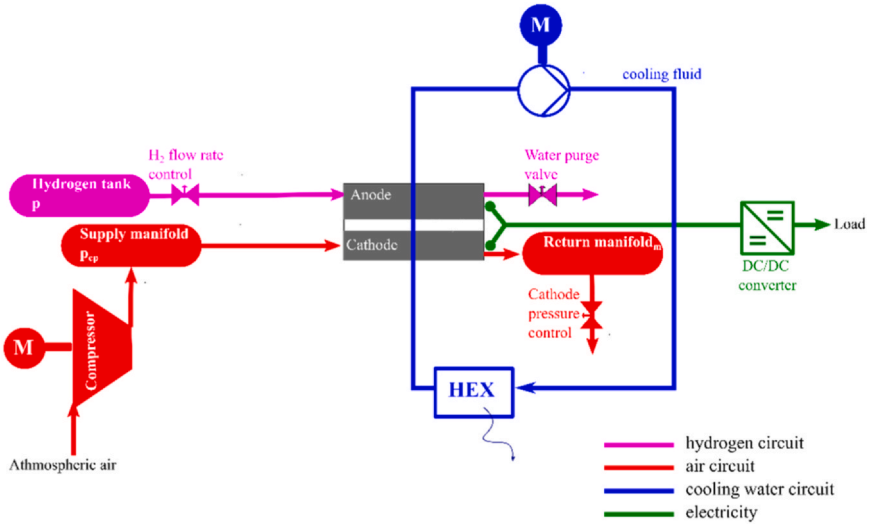


**Fig. 2.** Typical balance of plant of an aeronautic fuel cell system (Donateo, 2023).

compressed using an electric motor before entering the cathode supply manifold. The pressure at the cathode can be regulated through a valve located downstream of the return manifold. The electric power needed by the motor-compressor is normally obtained by the stack, except for the startup procedure when an auxiliary battery is needed.

Each machine in the balance of plant, and in particular the compressor, determines a parasitic power from the stack. The net power of a fuel cell system can be written as:

$$P_{net} = V_{st} I_{st} \eta_{DC-DC} - P_{par} \quad (1)$$

Where $\eta_{DC-DC}$ is the efficiency of the DC-DC converter and $P_{par}$ is the parasitic power of the whole BOP.

### 2.1. Effect of altitude

It is well known that ambient temperature, pressure, and relative humidity varies with elevation. This affects the performance of a PEMFC and brings challenges for its thermal management because of the increased air velocity and volumetric flow rate required for the cooling of the stack (Barroso et al., 2015; Gong et al., 2022).

In a closed-cathode configuration, the reduction of density can be counteracted by increasing the pressure ratio of the compressor. However, this determines an increase of the parasitic power causing a reduction of the net power and efficiency. In a closed-cathode PEMFC with a rated power of 1.2 kW tested at an altitude of 1524 m, a drop in the power of 25 % compared to sea level was measured (Song et al., 2022). This is in line with the information reported in the manual of the tested PEMFC (Nexa Power Module User's Manual) where a power drop of 15 W for every 100 m increase in altitude and 10 watts for every degree Celsius is acknowledged. More details about numerical and experimental studies that analyze this effect can be found in (Donateo, 2023).

### 2.2. Hybridization topologies

The fuel cell and the secondary storage system in a hybrid electric power system can be connected to the electric load in a variety of possible topologies as shown in Fig. 3. They differ in efficiency, performance, compactness, and cost (Kabalo et al., 2010).

In a passive configuration, Fig. 3a, there is a direct connection between the battery and the fuel cell. A simple switch is used to connect or disconnect one of the two energy sources. The power distribution between the two sources is automatically regulated by the load through the voltage. The voltages of the two components must be accurately chosen according to which is the main power source, the battery or the fuel cell. In aerospace applications, the main source is the fuel cell therefore its nominal voltage is higher than that of the battery. As the load increases, the fuel cell voltage decreases until it reaches the value of the battery voltage. For higher loads, the battery and the fuel cell work at the same voltage and both generate electricity for the load. This kind of system is very simple but does not allow the output power to be actively regulated and special operating procedures are needed to avoid discrepancies in the current-voltage behavior of the battery and the fuel cell (Nishizawa et al., 2013). Moreover, the size of the fuel cell and the battery must be accurately chosen to avoid charging the battery at too high currents. A passive or direct system is adopted in the Antares project.

To obtain an active regulation, it is necessary to add at least one DC-DC converter thus obtaining the "semi-active" configurations of Fig. 3b and c. The main power source, the battery in Fig. 3b or the fuel cell in Fig. 3c, can directly provide power to the load avoiding the energy losses of the DC-DC converter. As already explained, in aerospace applications the main energy source is the fuel cell. Therefore, configuration c) should be adopted. However, fluctuations in the load negatively affect the fuel cell lifetime so the DC-DC converter is often allocated on the fuel cell side as in the ENFICA-FC project (Romeo et al., 2011), in (Geliev et al., 2019), and in (Mazzeo and Di Ilio, 2024).

An architecture adopting a unidirectional DC-DC converter for the fuel cell and a bidirectional DC-DC for the battery, Fig. 3d, is called "fully active". The output power of each power source can be actively regulated, allowing the implementation of complex energy management strategies that guarantee high efficiency (Zhang et al., 2006). However, this configuration requires a large space, increases the weight, and is penalized by the electric losses in the two DC-DC converters. "Fully active" configuration are used in UAVs (Liu et al., 2022; Boukoberine et al., ).

### 2.3. Hybridization degree

The hybridization degree is used to classify hybrid electric power systems, especially when the main energy source is fossil fuel, whose

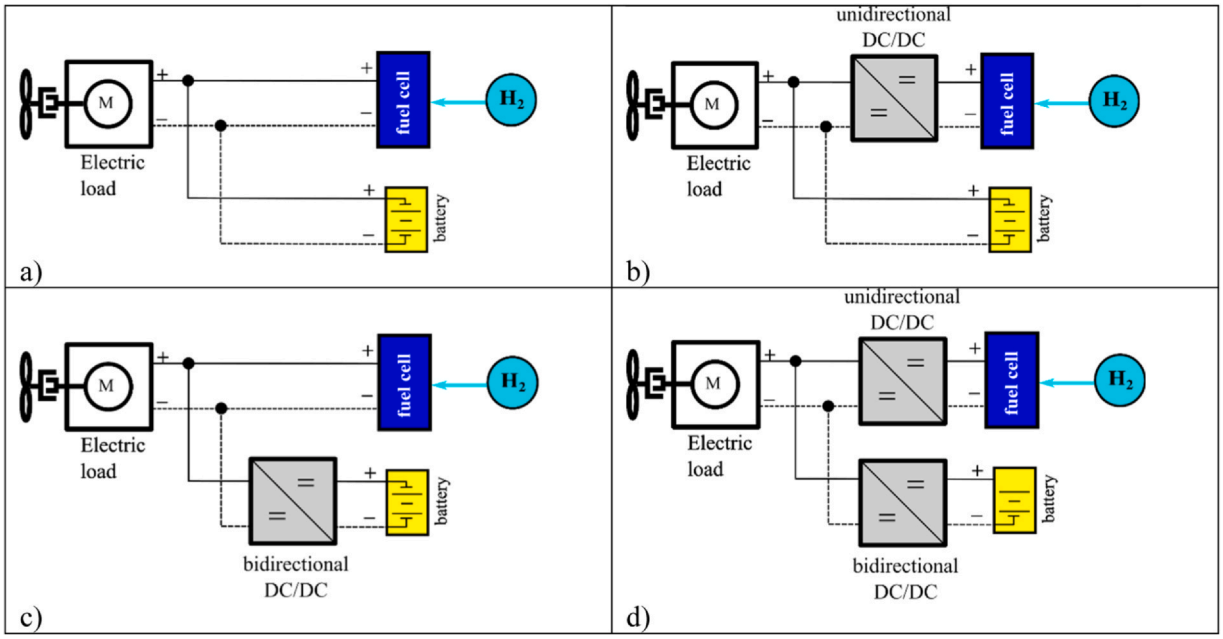


**Fig. 3.** Possible topologies of fuel cell hybrid electric power systems; a) passive or direct, b) semi-active with regulation of fuel cell voltage, c) semi-active with regulation of battery voltage, d) active configuration.

chemical energy is converted into mechanical power by an engine. In the aerospace field, two hybridization indexes have been introduced by Pornet et al (Pornet and Isikveren, 2015)., the power hybridization degree $H_P$ and the energy hybridization degree $H_E$. They are defined as:

$$H_P = \frac{P_{EM,nom}}{P_{TOT}} = \frac{P_{EM,nom}}{P_{ICE,nom} + P_{EM,nom}} \quad (2)$$

$$H_E = \frac{E_{batt,nom}}{E_{tot}} = \frac{E_{batt,nom}}{E_{batt,nom} + E_{fuel}} \quad (3)$$

In Eq. (2), $P_{EM,nom}$ and $P_{ICE,nom}$ are the nominal power of the electric machines and the engines, respectively. Their sum is the total installed power $P_{TOT}$. Similarly, in Eq. (3), $E_{batt}$, is the nominal energy of the battery and $E_{fuel}$ the energy stored in the fuel tanks.

In hydrogen hybrid electric power systems, however, the sizing is not expressed in terms of $H_E$ and $H_P$ because a fuel cell-only power system is rarely considered. In this case, the benchmark for hybridization is a battery-only configuration. Therefore, the power hybridization degree should be expressed as:

$$H_P = \frac{P_{FC,nom}}{P_{FC,nom} + P_{batt,nom}} = 1 - \frac{P_{batt,nom}}{P_{FC,nom} + P_{batt,nom}} \quad (4)$$

where $P_{FC,nom}$ is the nominal power of the fuel cell.

This parameter coincides with the fuel cell contribution to the takeoff power, $x_{FC}$, that is used here for the retrofitting analysis:

$$x_{FC} = \frac{P_{FC,nom}}{P_{takeoff}} \bullet 100 \quad (5)$$

where $P_{takeoff}$ is the electric power required by the electric motor during takeoff (which is the most demanding phase of the flight).

### 2.4. Batteries for aircraft electrification

Lithium batteries are nowadays used in all-electric and hybrid-electric power systems. However, the family of lithium batteries is quite broad, and, consequently, battery specifications like energy density, cycle life, power density, etc. have a large range of variation (Jarry et al., 2021b). Actually, there is a trade-off between energy density and maximum battery power/current, so batteries designed to achieve very high values of energy density are characterized by limited discharging currents and, consequently, low power density (Thomas, 2009; Donateo and Spedicato, 2017; Miazga et al., 2021). By combining different anode, cathode, separator, and electrolyte materials it is possible to improve one of the performance indexes at the expense of the other.

There are six main technologies commercially adopted for lithium-ion batteries (Wang et al., 2021a):

- LCO ($LiCoO_2$ – Graphite)
- LMO ($LiMn2O_4$ – Graphite)
- NCA ($LiNiCoAlO_2$ – Graphite)
- NMC ($LiNiMnCoO_2$ – Graphite)
- LFP ($LiFePO_4$ – Graphite)
- LTO (various - $Li_4Ti_{15}O_{12}$)

A further increase in compactness and discharge current can be obtained by adopting the lithium-polymer technology (Li-po). Li-po batteries differ from their lithium-ion counterpart in that a polymer electrolyte is used instead of a liquid lithium-salt. This kind of battery is lighter and more flexible than standard Li-ion cells but it is more prone to explosion and must be charged under controlled conditions.

The specifications of each battery technology, as found in the scientific literature ( (Geliev et al., 2019); ANON, 2023b, 2023c, 2023d; Camargos et al., 2022; ANON, 2023e, 2023f), are reported in Table 1 where GED and VED are acronyms for Gravimetric Energy Density and Volumetric Energy Density, respectively. About safety, which is a very important criterion in the aerospace field, the thermal runaway temperature is adopted as a measure of battery safety in Table 1. The higher this temperature, the safer the battery.

The most interesting chemistries are the LFP for their higher power density and higher safety and the NCA for their very high energy density. Li-po are the best in terms of power density but cannot be charged on-board. NMC batteries represent the best compromise between power density and energy density.

Another criterion for selecting the battery is the suitability to charge the battery on-board. From this point of view, LTO batteries are the best (and also guarantee the highest lifespan) but they are also the most expensive.

### 2.5. Energy management strategies

During the other phases of flight, hybrid electric power systems guarantee a degree of freedom in the power split between the fuel cell and the battery that is exploited by adopting a suitable energy management strategy (EMS). The goal of the EMS is to minimize a merit function, generally, the fuel consumption, while maintaining the desired state of charge of the battery and respecting the limits of each power source. Note that the hybridization degree refers to the installed power while the EMS decides how the two power sources are used along the flight mission for a given hybridization degree.

EMSs can be classified into heuristics and optimization-based (Onori et al., 2016; Pornet and Isikveren, 2015). In applications with a fast dynamic of the load like road transportation (Onori et al., 2016; Mercier et al., 2023) and small unmanned, aerial vehicles, (Boukoberine et al., ), advanced EMSs have been proposed. In reverse, very simple rule-based heuristic EMSs are commonly adopted in the preliminary design of hybrid electric power systems with fuel cells for ultralight and light aviation (Mazzeo and Di Ilio, 2024) due to the almost constant request of power during large part of the flight.

About the battery, it is possible to adopt Charge Depleting (CD) strategies (where the battery is discharged during the mission and charged, externally, after the flight) or Charge Sustaining (CS) methods, where the battery is charged on-board using the fuel cell so that no external charging is required (Onori et al., 2016).

### 2.6. Examples of fuel cell-powered aerial vehicles

In the past, fuel cells were employed in general aviation only as Auxiliary Power Units in More Electric Aircraft configurations

**Table 1**
Range of performance indexes of different li-ion technologies at the cell level.

| Battery type | Voltage (V) | GED (Wh/kg) | VED (Wh/L) | Discharging rate | Charging rate | Lifespan | Thermal runaway |
|---|---|---|---|---|---|---|---|
| LCO | 3.6 | 140-200 | 400 | 0.7 C – 1 C | 0.7 C – 1 C | 500-1000 | 150 °C |
| LMO | 3.7 | 100-150 | 350 | 1 C – 10 C | 0.7 C – 3 C | 300-700 | 250 °C |
| NCA | 3.6 | 200 - 260 | 550 | 1 C – 3 C | 0.7 C – 1 C | 500 - 1000 | 150 °C |
| NMC | 3.7 | 150 - 230 | - | 1 C – 10 C | 0.7 C – 1 C | 1000- 2000 | 210 °C |
| LFP | 3.2 | 90 - 170 | 350 | 1 C – 25 C | 1 C | > 4000 | 270 °C |
| LTO | 2.2 | 35-100 | 177 | 4 C – 10 C (30 C pulsed) | 1 C – 5 C | > 20000 | Very high |

**Table 2**
List of projects adopting PEMFCs for manned aerial vehicles.

| Project | Aircraft | Takeoff requirements | FC power | Cooling type | Hydrogen storage | Source |
|---|---|---|---|---|---|---|
| **Boeing Phantom** | Motor glider | 770 kg | 20 kW | Liquid-cooled | Pressurized at 350 bar | (Lapeña-Rey et al., 2007) |
| **ENFICA-FC** | Ultralight | 554 kg/35 kW | 20 kW | Liquid-cooled no fan | Pressurized | (Romeo et al., 2011) |
| **Sigma-4** | Ultralight | 650 kW / 65 kW | 35 kW | Liquid-cooled | Pressurized | |
| **Antares DLR-H2** | Motor glider | 42 kW | 3 × 10 kW | Air-cooled HT vs liquid-cooled LT | Pressured at 350 bar | (Rathke et al., 2014) |
| **H2fly Pipistrel HY4 2016** | 4 pax | N.A. | 4 × 10 kW | Turbo-cooled HT | Liquefied | (Gao et al., 2022) |
| **ZeroAvia HyFlyer I** | 6 pax | N.A. | 250 kW | Air-cooled high-temperature | N.A. | (ANON, 2023g) |
| **ZeroAvia HyFlyer II** | 19 pax | 560 kW | 4 × 140 kW | Liquid-cooled | Liquefied | (Kasim and Marek, 2022) |

(Motapon et al., 2013). Since the design of the first hydrogen-powered aerial vehicle (Bradley et al., 2007), many fuel cell systems have been proposed for Unmanned Aerial Vehicles (UAVs) (Suewatanakul et al., 2022), ultralight manned aviation and lightweight helicopters for Urban Air Mobility. A selection of projects related to light and ultralight aviation is reported in Table 2.

Liquid-cooled PEMFCs are generally adopted in this application (ENFICA-FC (Romeo et al., 2011), Sigma-4 (Geliev et al., 2019)). However, there has been an effort to extend the application range of air-cooled fuel cells beyond 6 kW (Wright and Aaltonen, 2022) by adopting edge-cooling and phase-change cooling devices (Kim and Kwon, 2012; Pratt et al., 2007; Wang et al., 2021b; Chen et al., 2017; Tolj et al., 2020).

High-temperature proton exchange membrane fuel cells (HT-PEMs) that work with temperatures in the range of 100 °C-200 °C are proposed in the Antares DLR-H2 project (Rathke et al., 2014). The advantages of HT-PEMs are the lack of water management systems for humidification, and the lower requirements in terms of hydrogen purity. On the other hand, they are more expensive and require a longer start-up time and hybridization degree, i.e., a larger battery.

Another option is the modular construction of fuel cell systems (Rathke et al., 2014) by connecting more lightweight air-cooled devices in series or parallel, like in the case of the Antares project where three modules are connected to reach the nominal output of 30 kW (Rathke et al., 2014).

### 2.7. Sizing methodologies

The sizing methodologies proposed in the scientific literature can be classified into retrofitting techniques (Mazzeo and Di Ilio, 2024) and conceptual design methods (Suewatanakul et al., 2022; Moffitt et al., 2006; Donateo and Çinar, 2022). A parametric analysis that considers three different levels of the fuel cell power is performed in (Mazzeo and Di Ilio, 2024) where the size of the battery is kept constant while the amount of hydrogen stored on board is reduced with increased fuel cell power to keep the takeoff mass.

In retrofitting studies, the sizing of the fuel cell is usually performed by choosing the nominal power of the fuel cell equal to or slightly higher than the cruise power, while the battery is sized to generate the missing energy at takeoff and climb, with a further energy content to provide the energy necessary for an emergency landing in case of fuel cell failure (Miazga et al., 2021). For the sizing of the Boeing Phantom demonstrator airplane, the authors of (Lapeña-Rey et al., 2007) used the minimum power for cruise at a given altitude and speed as the minimum requirement for the fuel cell. The Nichel/Cadmium battery was sized according to the desired values of the rate of climb at its continuous max power.

In (Lapeña-Rey et al., 2007) the hydrogen vessel was sized to ensure an endurance of 30 min. At take-off, the electric motor receives half power from the battery and half from the fuel cell. In case of fuel cell failure during takeoff and climb, the battery can work at its peak power to perform an emergency landing.

The design of an electric propulsion system for an ultralight manned aircraft based on a retrofitting approach is proposed also in (Geliev et al., 2019), where the target was not to exceed the aircraft's maximum takeoff mass. The fuel cell was sized according to the cruise power plus 5 kW for the on-board needs. The battery was designed to deliver 30 kW during the 3 min required for takeoff and climb. The electric motor had a total rated power of 30 kW and a peak power of 60 kW. The sizing was performed with a model-based approach to estimate the efficiency of the fuel cells in the different operating modes. The mass of hydrogen stored in the vessel, 2.55 kg, was chosen to allow an hour of flight. A commercial hydrogen vessel with a storage pressure of 392 bar, an internal volume of 100 L, and a mass of 56 kg was selected to achieve the desired mass of hydrogen.

A model-based preliminary design methodology for a hybrid regional aircraft assisted by a battery was proposed in (Sparano et al., 2023) while an optimization method was adopted in (Moffitt et al., 2006) for the design of a hydrogen-powered unmanned vehicle with hydrogen as the only energy source (no battery). The two competitive goals of the optimization (range and takeoff mass) were combined in a global utility criterion. The design variables included the specifications of the fuel cell, the motor, the propeller, and the fuselage geometry.

Regarding the sizing of the power system, in the investigation of Miazga et al (Miazga et al., 2021). the charging of the battery during flight was barred because the charging process is less efficient and can cause high thermal losses, particularly at high current.

To the authors' knowledge, another shortcoming of previous studies is that the drop in fuel cell power with increasing flight altitude is disregarded in the sizing of the power system.

### 2.8. Original contribution

The innovative aspects of the procedure proposed in the present investigation are:

- The minimization of both the weight and occupied space of the power system.
- The use of twelve different missions with an assortment of climb rates, cruise speed and altitude, propeller pitch and efficiency, etc.
- The use of datasheet specifications for the main components of the power system.
- The comparison of five types of lithium battery technologies in terms of power density, energy density, discharge and charge current, cost, and safety.
- The scale-up of the fuel cell nominal power to account for the performance loss at the flight altitude.

A simple energy management strategy compatible with a passive configuration is used for the sizing process.

## 3. The seagull

The goal of the project is the development of a zero-emission propulsion architecture by retrofitting the Novotech Seagull aircraft. The

| *Property* | *Value* |
|---|---|
| Wingspan | 10.5 m |
| Wing area | 13.5 $m^2$ |
| Max Gross Weight | 700kg |
| Maximum Zero Fuel Weight | 650 kg |
| Maximum Baggage Weight | 20 kg |
| Pay weight | 80kg |
| Power Loading | 6.5 kg/HP |
| Engine type | Rotax 912 ULS2 |
| Engine power | 100hp @ 5800rpm |
| Fuel tank capacity | 70 L (50kg) |

**Fig. 4.** Picture and main specifications of the Seagull.

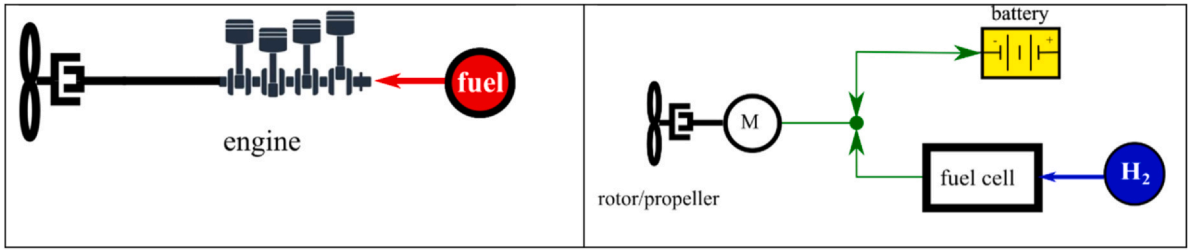


**Fig. 5.** Original (left) and proposed (right) power systems.

Seagull is a two-seat high-wing amphibian vehicle equipped with a piston-prop configuration. The main specifications of the Seagull and its propulsive system are reported in Fig. 4.

The original and proposed power systems are depicted in Fig. 5. In the original configuration, a piston engine is used to generate the required thrust and to supply 600 W for on-board services by means of a generator. In the retrofitting, the engine and the fuel tank are replaced by a hybrid electric propulsion system consisting of an electric machine connected to the propeller by a reduction gear, a lithium battery, a PEMFC, and a compressed hydrogen vessel. This system produces all the power necessary for the flight and the on-board services. Note that the term fuel cell in the scheme of Fig. 5 is meant to include the stack and its balance of the plant (BOP).

The mass of the engine inclusive of the fuel system, liquids, and fuel is equal to 152 kg (Geliev et al., 2019) and the space occupied by the fuel tank is 70 L. In the retrofitting of the Seagull, the mass of the new powertrain must be controlled not to exceed the max gross weight. After a careful analysis of the Seagull architecture, a total mass of 200 kg is assumed as the target for the design of the new propulsive system. As for the occupied space, an analysis of the space available in the aircraft led to the choice of a target value of 200 L for the whole system.

### 3.1. Reference missions

Twelve different missions named #01 #02, …, and #12 were proposed by Novotech as representative of the typical use and setting of the Seagull. Each mission consists of up to six phases or flight segments (takeoff, climb 1, cruise 1, climb 2, cruise 3, and descent) as reported in Fig. 6. The missions differ not only for cruise speed, propeller pitch setting, altitude, and climb rate (as shown in Table 3), but also for the duration of the flight segments. In two cases (#03 and #04) a degradation of the propeller efficiency is considered. The twelve missions can be classified into long (from #01 to #05) and short missions (#06 - #12) according to their total flight time which is 90 or 30 min, respectively. The total range is 225 km for the first four missions, 256 km for #05, 85 km for missions from #06 to #0.8, and 75 km for the last three.

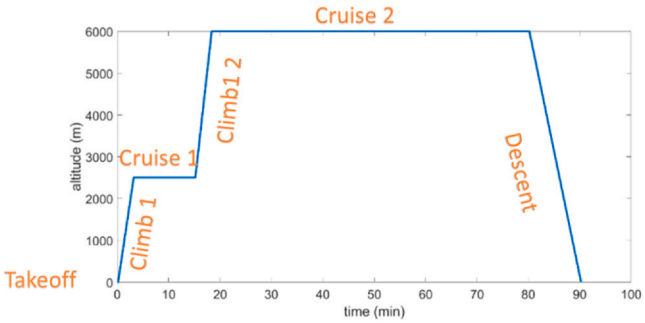


**Fig. 6.** The six phases of the flight.

At takeoff, the average thrust $\bar{T}$ can be calculated from the average value of the advance ratio $\bar{J}$ (computed as the mean value between the beginning of the takeoff, where $J = 0$, and the lift-off point where $J = \frac{V_{lo}}{nD_p}$ with $V_{lo}$ the lift-off speed). The average acceleration $\bar{a}$ is given by:

$$\bar{a} \approx g\frac{\bar{T}}{W_{TO}} \tag{6}$$

Where $W_{TO}$ is the takeoff weight. The average takeoff time $\bar{t}$ is calculated as:

$$\bar{t} = \frac{V_{lo}}{\bar{a}} \tag{7}$$

The total thrust during climb is (McCormick, 1995):

$$T_{climb} = \frac{RC \bullet W + D \bullet V}{V} \tag{8}$$

Where $D$ is the drag force, $RC$ is the rate of climb, $W$ and $V$ are the weight and the true airspeed of the aircraft. The same equations can be used for the descent phase. Note that in case of electric propulsion, the weight does not change during the mission.

**Table 3**
Specifications of the missions.

| mission | Pitch setting | Lift-off speed (m/s) | Rate of climb 1 (m/s) | Rate of climb 2 (m/s) | Rate of descent (m/s) | Cruise speed (m/) | Cruise 1 / 2 altitude (ft) | Total time (minutes) | Propeller efficiency correction |
|---|---|---|---|---|---|---|---|---|---|
| #01 | 18.5 | 25 | 4.2 | 5.87 | -3.03 | 47.2 | 2500 /6000 | 90 | |
| #02 | 17.5 | 25 | 3.7 | 5.18 | -2.67 | 41.7 | 2500/6000 | 90 | |
| #03 | 18.5 | 25 | 4.2 | 5.87 | -3.03 | 47.2 | 2500/6000 | 90 | -20 % |
| #04 | 17.5 | 25 | 3.7 | 5.18 | -2.67 | 41.7 | 2500/6000 | 90 | -20 % |
| #05 | 18.5 | 25 | 5.79 | - | -3.03 | 47.2 | 2500 | 90 | |
| #06 | 18.5 | 25 | 5.79 | - | 3.03 | 47.2 | 2500 | 30 | |
| #07 | 21.5 | 25 | 5.75 | - | -3.03 | 41.7 | 6000 | 30 | |
| #08 | 18.5 | 25 | 5.79 | - | -3.03 | 47.5 | 6000 | 30 | |
| #09 | 17.5 | 25 | 5.08 | - | -2.67 | 41.7 | 6000 | 30 | |
| #10 | 17.5 | 25 | 5.08 | - | -2.67 | 41.7 | 2500 | 30 | |
| #11 | 21.5 | 25 | 5.08 | - | -2.67 | 41.7 | 6000 | 30 | |
| #12 | 21.5 | 25 | 5.08 | - | -2.67 | 41.7 | 2500 | 30 | |

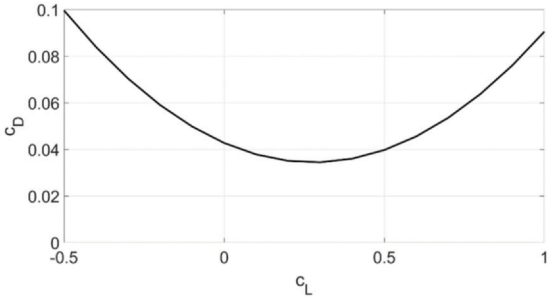


**Fig. 7.** Polar of the Seagull.

At cruise, the thrust is equal to the drag force ($T_{cruise} = D$), so:

$$T_{cruise} = \frac{1}{2} c_D \rho S V^2 \tag{9}$$

In this equation, ρ is the air density which decreases as the flight altitude increases, S is the wing area, and $c_D$ is the drag coefficient that can be obtained from the lift coefficient using the polar curve of Fig. 7.

The lift coefficient $c_L$can be calculated from the lift force that counterbalance the weight:

$$L = W = \frac{1}{2} c_L \rho S V^2 \tag{10}$$

From the values of true airspeed $V$ and air density $\rho$ calculated at the flight altitude, it is possible to obtain the advance ratio of the propeller in each flight segment:

$$J = \frac{V}{nD_p} \tag{11}$$

Where $n$ is the propeller speed in rps and $D_p$ is the propeller diameter.

Once the pitch setting is selected, the corresponding values of thrust coefficient $C_T(J) = T/(\rho n^2 D_p^4)$, power coefficient $C_p(J) = P/(\rho n^3 D_p^5)$, and efficiency ($\eta_P = TV/P$) are computed from the propeller maps (Fig. 8).

The electrical power required by each segment $j$ of the mission can be calculated as:

$$P_{el}(j) = \frac{T(j) \bullet V(j)}{\eta_P \eta_T \eta_{EM}} + P_{aux} \tag{12}$$

Where $\eta_T$ is the efficiency of the speed reduction gear and $\eta_{EM}$ is the efficiency of the electric motor inclusive of its controller and inverter (whose efficiency is assumed 96.6 % as in (Miazga et al., 2021). $P_{aux}$ is the electric consumption of on-board auxiliaries (600 W).

The specifications of the twin electric machines selected for the retrofitting are reported in Table 4 while their efficiency map is shown in Fig. 9. The very high peak power (124 kW x 2) of the electric machines allows the reduction of the take-off time to 10 s

By applying Eq. (15), the electric power profiles of Fig. 10 are obtained for each phase of the twelve missions.

## 4. The sizing methodology

A parametric analysis is performed for the sizing of the hybrid electric power system of Fig. 5b. The design variables for the minimization of weight and occupied space are the battery technology, $ID_b$, and the fuel cell contribution to the takeoff power of the mission, $x_{FC}$,

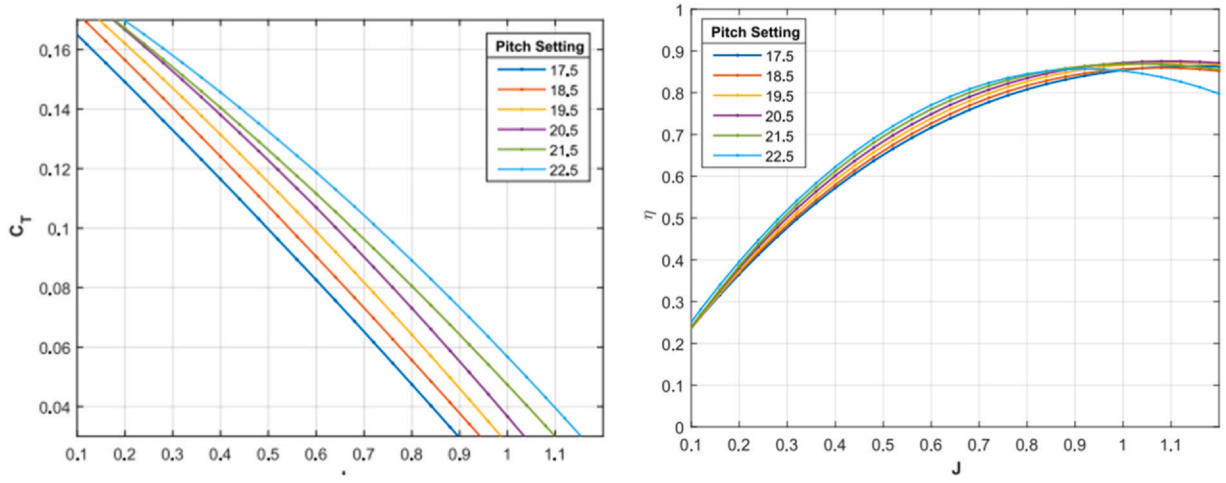


**Fig. 8.** Propeller thrust coefficient (left) and efficiency (right) as a function of advance ratio J and pitch setting.

**Table 4**
Specifications of the electric motor.

| Parameter | Value |
|---|---|
| Peak power | 124 kW |
| Continuous power | 75 kW |
| Peak torque | 230 Nm |
| Continuous torque | 130 Nm |
| Max speed | 6500 rpm |
| Base speed | 5000 rpm |
| Operating voltage | 50-710 V |
| Weight | 13.5 kg |
| Volume | 3.5 L |

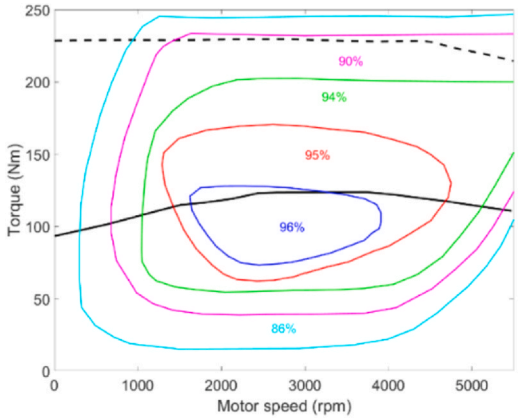


**Fig. 9.** Torque limits (black line) and efficiency map (contour lines) of the electric motor.

which is increased from 0 % (battery-only configuration) to 100 % (fuel cell-only configuration).

The volume and mass of the whole power system is calculated, for each value of $x_{FC}$ and $ID_b$ as:

$$M_{tot}(x_{FC}, ID_b) = M_{batt} + M_{FC} + M_{H_2tank} \tag{13}$$

The mass of the fuel cell is considered inclusive of BOP, electronic converters and control systems.

The total volume is given by:

$$V_{tot}(x_{FC}, ID_b) = V_{batt} + V_{FC} + V_{H_2tank} \tag{13}$$

### 4.1. Sizing the fuel cell

The fuel cell mass and volume are calculated from preassigned values of gravimetric power density (GPD) and volumetric power density (VGP) as:

$$M_{FC}(x_{FC}) = \frac{P_{FC,nom}}{GPD_{FC}} \tag{14}$$

$$V_{FC}(x_{FC}) = \frac{P_{FC,nom}}{VPD_{FC}} \tag{15}$$

Where the nominal power of the fuel cell is corrected to account for the loss of power at the cruise altitude:

$$P_{FC,nom} = \frac{x_{Fc}}{100} \bullet \frac{P_{takeoff}}{1 - 1.25 \bullet 10^{-4} \quad h_{\max}} \tag{16}$$

Where $h_{\max}$ is the maximum altitude of the mission. The correction term $(1 - 1.25 \bullet 10^{-4} \quad h_{\max})$ was obtained by assuming a loss of 1.25 % of power every 100 m of altitude (Nexa Power Module User's Manual).

In each phase of the flight, the power of the fuel cell and the battery can be chosen with the constraint of satisfying the following equation:

$$P_{FC}(i) + P_{batt}(i) = P_{el}(i) \tag{17}$$

where $P_{el}(i)$, $P_{batt}(i)$, and$P_{FC}(i)$ are the total electric power, the battery power, and the fuel cell power of the mission phase $i$.

Two different energy management strategies (with and without battery charging) are proposed and compared. In the first strategy, named "with charge", the fuel cell works at constant power during the whole flight. The battery is charged if the fuel cell power exceeds the request for electricity from the motor, provided this is compatible with the charging limits of the battery. Otherwise, the battery power charge (negative in our convention) is set equal to the maximum charging power ($P_{batt,ch}(i) = -I_{\max,ch} V_{batt}$), and the fuel cell power is adapted to match the electric power request. In the second strategy, "w/o charge", the procedure is the same but the battery cannot be charged during the flight.

Note that these simple energy management strategies are compatible with a passive hybrid electric configuration where the power split between the fuel cell and the battery is regulated by the fuel cell voltage that decreases with load.

### 4.2. Sizing the hydrogen tank

The flow rate of hydrogen ($H_2FR$) in each phase of the mission is calculated as:

$$H_2FR(i) = \frac{P_{FC}(i)}{\eta_{FC} HHV_{H_2}} \tag{18}$$

Where $\eta_{FC}$ is the average efficiency of the fuel cell and $HHV_{H_2}$is the heating value of hydrogen.

By integrating $H_2FR$ over the mission is is possible to obtain the overall mass of hydrogen consumed in the mission:

$$M_{H_2} \quad = \sum_{i=1}^{6} H_2FR(i)\Delta t(i) \tag{19}$$

Where $\Delta t(i)$ is the time duration of flight phase $i$.

The mass of hydrogen is used to define the mass of the hydrogen tank by means of the storing efficiency $\eta_{stor}$:

$$M_{H_2tank} = M_{H_2}/\eta_{stor} \tag{20}$$

$V_{H_2tank}$ is calculated as:

$$V_{H_2tank} = \frac{\sum_{i=1}^{6} P_{FC}(i)\Delta t(i)}{\eta_{FC} \bullet VED_{H_2}} \tag{21}$$

Where $VED_{H_2}$is the volumetric energy density of hydrogen at the storing conditions.

According to the limits of the pressure regulator, the tank could not be completely depleted during the operation. For this reason, a reserve for five minutes of fuel cell operation can be considered (Rathke et al., 2014).

### 4.3. Sizing the battery

The energy that the battery can provide during the flight can be calculated from its nominal specifications as:

$$E_{batt} = DOD \bullet C_{nom} \bullet V_{batt} \tag{22}$$

Where $C_{nom}$ and $V_{batt}$ are the nominal values of capacity and voltage of the battery pack, respectively. $DOD$ is the Depth of Discharge, i.e., the maximum percentage of a battery's capacity (usually expressed in Ah) which is removed from the battery in normal operation. DOD is not to be confused with the State of Charge (SOC) which is the percentage of the capacity which is currently removed from the battery. The DOD is usually limited to a value below 100 % to preserve the health of the battery and reduce the degradation of its performance.

The power of the battery is limited by the need to avoid deterioration and damage. The maximum continuous battery power in discharge and in charge are given by:

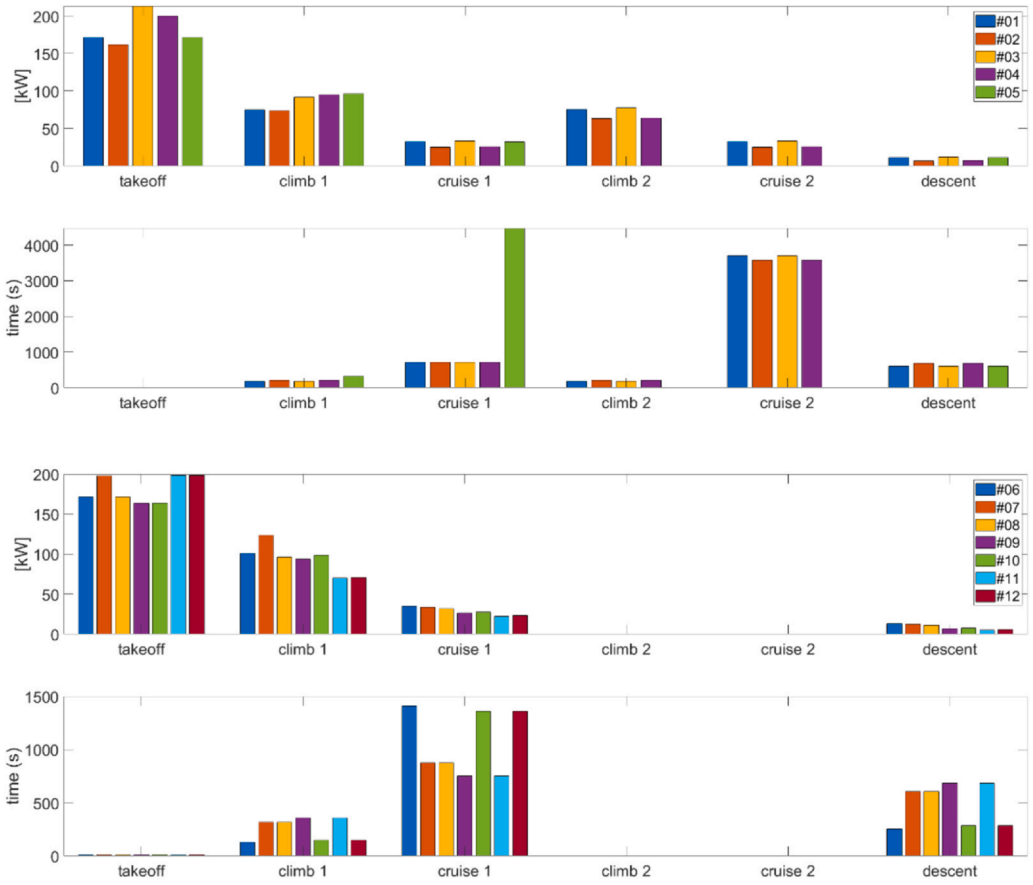


**Fig. 10.** Requests of power in the six phases of the missions.

$$P_{max,dis} = I_{max,dis} \bullet V_{batt} \tag{23}$$

$$P_{max,ch} = I_{max,ch} \bullet V_{batt} \tag{24}$$

The maximum current in discharge, $I_{max,dis}$, and charge, $I_{max,ch}$, are expressed as multiples of the nominal capacity $C_{nom}$:

$$I_{max,dis} = C_{rate,dis}(ID_b) \bullet C_{nom} \tag{25}$$

$$I_{max,ch} = C_{rate,ch}(ID_b) \bullet C_{nom} \tag{26}$$

Where $C_{rate,dis}$ and $C_{rate,ch}$ are specifications usually reported in the datasheets.

Like the motors, the battery can be discharged, for a short time, at a current larger than $I_{max,dis}$ that is named "burst current". However, this operating mode is not adopted here to avoid battery damage.

In terms of power, the battery must be able to complement the fuel cell in each phase and, in particular, at takeoff:

$$P_{batt,nom} = \left(1 - \frac{x_{Fc}}{100}\right) \bullet P_{takeoff} \tag{27}$$

The energy that the battery releases or receives in each phase $i$ is calculated by multiplying the power by the flight time and converted $Wh$. The range of variation of battery energy is obtained from Eq. (32) and shown in Fig. 11 with the red arrow.

$$\Delta E_{batt} = \frac{\max(E_{batt}(i)) - \min(E_{batt}(i))}{3600} \tag{28}$$

A tentative value of the nominal size of the battery is then calculated as:

$$E_{batt,nom,in} = \frac{\Delta E_{batt}}{DOD} \tag{29}$$

By setting the nominal voltage of the battery, $V_{batt}$, it is possible to obtain the tentative value of the nominal capacity:

$$C_{nom,in} = E_{batt,nom,in}/V_{batt} \tag{30}$$

However, this equation is not sufficient to size the battery. As already explained, it is necessary to verify that $-P_{max,ch} \le P_{batt}(i) \le P_{max,dis}$ Therefore, the following constraints are to be met:

$$I_{max,batt}(i) = \frac{P_{max,dis}}{V_{batt} \bullet C_{nom}} = \frac{P_{batt}(1)}{V_{batt} \bullet C_{nom}} \le C_{rate,dis}(ID_b) \tag{31}$$

And

$$|I_{min,batt}(i)| = \frac{|P_{max,ch}|}{V_{batt} \bullet C_{nom}} = \frac{|P_{batt}(6)|}{V_{batt} \bullet C_{nom}} \le C_{rate,ch}(ID_b) \tag{32}$$

Eq.(36) is used within the energy management strategy to correct the power of the battery and the fuel cell when this constraint is not satisfied.

According to the value of $x_{FC}$, the strictest condition for the sizing of the battery can be either the energy requirement or the power requirement. Therefore, the nominal capacity of the battery is selected as:

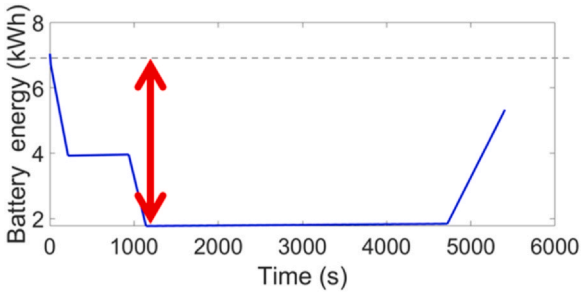


**Fig. 11.** Typical trend of battery energy in the case of on-board charge. The red arrow indicates the range $\Delta E_{batt}$ used to size the battery.

**Table 5**
List of the parameters assumed for the fuel cell system and the hydrogen vessel.

| Component | Variable | Description | Value | Source |
|---|---|---|---|---|
| Fuel cell | $GPD_{FC}$ | Gravimetric power density of the fuel cell | 300 W/kg | Arco Fuel Cells datasheets |
| | $VPD_{FC}$ | Volumetric power density of the fuel cell including BOP | 300 W/L | Arco Fuel Cells, datasheets |
| | $\eta_{FC}$ | Fuel cell efficiency | 45 % | Arco Fuel Cells Datasheets, (Kasim and Marek, 2022) |
| Hydrogen vessel | $HHV_{H_2}$ | Higher Heating Value of hydrogen | 39000 Wh/kg<br>35000 Wh/kg | (Rubio et al., 2023) |
| | $\eta_{stor}$ | Hydrogen storage efficiency (pressurized tank at 700 bar) | 5.5 % | (Geliev et al., 2019; Jarry et al., 2021a) |
| | $VED_{H2}$ | Volumetric energy density of compressed hydrogen at 700 bar | 1300 Wh/L (40 kg/m$^3$) | (Geliev et al., 2019; Taccani et al., 2020) |

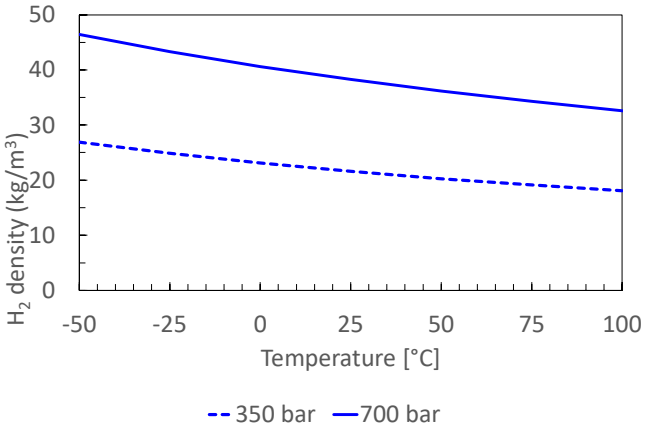


**Fig. 12.** Density of hydrogen vs temperature at different storing pressures.

$$C_{nom} = \max\left(\frac{\Delta E_{batt}}{DOD \bullet V_{batt}}, \quad \frac{P_{batt}(1)}{V_{batt} \bullet C_{rate,dis}}\right) \tag{33}$$

The mass and the volume of the battery can be finally calculated:

$$M_{batt}(x_{FC}, ID_b) = \frac{E_{batt}(x_{FC})}{GED_{batt}(ID_b)} = \frac{C_{nom} \bullet V_{batt}}{GED_{batt}(ID_b)} \tag{34}$$

$$V_{batt}(x_{FC}, ID_b) = \frac{E_{batt}(x_{FC})}{VED_{batt}(ID_b)} = \frac{C_{nom} \bullet V_{batt}}{VED_{batt}(ID_b)} \tag{35}$$

Thanks to the limited calculation time of the proposed procedure, a full space exploration was used; $x_{FC}$ was increased from 0 % to 100 % with a step of 0.1 % and the battery ID from 1 to 5. Moreover, two cases were run for each mission, with and without on-board charge.

### 4.4. Technological scenario

The technological specifications of the fuel cell and the hydrogen tank adopted in this investigation are summarized in Table 5 together with their reference.

According to NASA (Datta, 2021), the specific power density of a state-of-the-art fuel cell with a power of 20 kW ranges between 0.3 and 1 kW/kg. However, this parameter depends on the size of the fuel cell and manufacturer (ANON, 2023h) and on the complexity of the BOP (Geliev et al., 2019). According to Geliev et al (Geliev et al., 2019)., the specific power of commercial PEMFCs is 1 kW/kg with examples of 2–2.5 kW/kg stacks (Jarry et al., 2021a). A conservative value of 0.6 kW/kg is considered in (Mazzeo and Di Ilio, 2024) while the specific power of the PEMFC, including all the masses that compose the hydrogen line (converter, fuel cell, storage system, and fuel) is 340 W/kg in (Mazzeo and Di Ilio, 2024). The overall weight of the BOP in a 30 kW liquid-cooled PEMFC was found to be (Geliev et al., 2019) increases the mass of a 30 kW stack by 16.7 %, while the mass of the air supply system is about 50 % of the total mass. The fuel cell stack contributes only 30 % of the overall volume, the rest being due to its BOP. The volume of the electronic converters is also taken into account in that study.

About the space occupied by the fuel cell systems, the total value can be deduced from the stack volume by considering a correction factor equal to 1.5 and 3 for air-cooled and liquid-cooled FCs respectively (WAN, 2015). In (Onori et al., 2016), a volumetric power density of 0.64 kW/L is assumed for a liquid-cooled fuel cell for automotive applications, on the base of existing fuel cell vehicles. The nominal power of the fuel cell is varied between 40 kW and 80 kW. From personal communication and datasheets of commercial liquid-cooled fuel cells, a gravimetric density of 300 W/kg and a volumetric of 300 W/L are assumed for the fuel cell overall system.

A conservative constant value of 45 % is assumed in this investigation for the net efficiency of the fuel cell. However, the efficiency of the fuel cell systems depends on the load. To this scope, a detailed model of the fuel cell system will be considered for further investigation.

The energy density of hydrogen increases with storing pressure and temperature, as reported in Fig. 12. According to (Geliev et al., 2019), the weight efficiency of 70 MPa pressurized hydrogen vessels ranges between 5 % and 5.8 %, while the volumetric efficiency is in the range 26–41 g/L which is coherent with the assumed value of 40 kg/m$^3$ for hydrogen density in Table 5.

The mass of a battery pack is larger than the sum of the masses of the cells connected in series and parallel, because of electric and mechanical connectors, the need for a cooling system, and the presence of a battery controller also called BMS or Battery Management System. To account for the additional mass and occupied space of the battery packs, the cell-based energy densities (Table 1) were divided by a factor of 1.3 (Arista et al., 2015) obtaining the data reported in Table 6. The values used for Li-po technology refer to batteries produced by Padre Electronics for helicopters, planes, and quadcopters.

**Table 6**
Values assumed in this investigation for battery parameters at pack level.

| $ID_b$ | Battery type | $GED_{batt}$ (Wh/kg) | $VED_{batt}$ (Wh/L) | $C_{rate,dis}$ | $C_{rate,ch}$ |
|---|---|---|---|---|---|
| 1 | NCA | **200** | **420** | 3 C | 1 C |
| 2 | NMC | 170 | 370 | 10 C | 1 C |
| 3 | LFP | 130 | 270 | **25 C** | 1 C |
| 4 | LTO | 77 | 136 | 10 C | **5 C** |
| 5 | LiPo | 100 | 210 | **70 C** | 1 C |

**Table 7**
Overall results of the parametric study (*min mass*) for the long missions.

| Mission | #01 | #02 | #03 | #04 | #05 |
|---|---|---|---|---|---|
| Battery type | LFP | LFP | LFP | LFP | LFP |
| Battery charge | yes | yes | no | yes | no |
| $x_{FC}$ (%) | 24 | 20 | 20 | 16 | 21 |
| FC size (kW) | 41.3 | 32.3 | 42.7 | 32 | 36.1 |
| $H_2$ (kg) | 2.7 | 2.1 | 2.6 | 2.1 | 2.6 |
| Bat. (kWh) | 5.3 | 5.2 | 6.8 | 7.8 | 7 |
| Tank (L) | 78 | 60.3 | 77.4 | 60.5 | 74.9 |
| Tot. Mass (kg) | 226.6 | 184.8 | 242.7 | 203.7 | 220.5 |
| Tot Vol. (L) | 235.3 | 187.3 | 245.2 | 196.1 | 221.3 |
| Sizing criterium | $\Delta E_{batt}$ | $P_{batt}$ | $P_{batt}$ | $\Delta E_{batt}$ | $\Delta E_{batt}$ |

## 5. Results

Table 7 and Table 8 summarizes the results of the application of the sizing procedure by showing the solution that minimizes the mass for each mission. This solution will be called henceforward "*min mass*". As for the volume, any hybrid configuration requires a higher volume than a battery-only configuration.

For long missions #01-#05 and the short mission #12, the powertrain that minimizes the mass is a hybrid configuration with a fuel cell and battery. The optimal fuel cell size for missions #01-#05 tendentially increases with electric power requested in cruise, but it is not proportional to it as shown in Fig. 13. The main reason for this nonlinear trend is the necessity to consider the power reduction with altitude. Note that the cruise altitude reaches 6000 ft in all long missions except mission #05. In fact, for this mission the optimal FC power is only 12 % higher than the cruise power. For mission #12, which is a short mission with a low altitude (2500 ft), the *min mass* configuration includes a very small fuel cell which is sized according to the descent power as shown in Fig. 14. In all the other flight phases, the main energy source is the battery.

The best battery technology for long missions #01–05 and #12 is the LFP. The battery is sized according to the energy criteria for missions #01, #04, and #12 and based on the power requirement for missions #02, and #03.

The targets of mass and volume can be strictly satisfied only for the short missions and for mission #02. However, the results for mission #04 can also be considered accepted since the mass target (200 kg) is infringed only by 1.8 %. Note that mission #04 has the same specification as mission #02 (Table 3), but accounts for a 20 % degradation in the propeller efficiency that causes high levels of power request in all phases of the mission (Fig. 10). The *min mass* configuration is almost the same for the two missions except for the battery which is 50 % larger in mission #04 than in mission #02. Similar considerations can be drawn for missions #01 and #03.

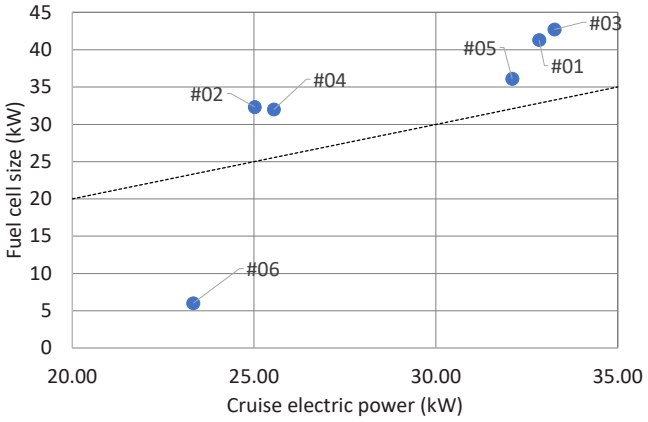


**Fig. 13.** Fuel cell size in the *min mass* configuration vs cruise electric power.

From the data of Fig. 10, it is possible to note that the main difference between mission #01 and #02 is the higher power during the cruise caused by the different setting of the pitch angle, while the climb power is only slightly higher for mission #01 because of the faster rate of climb. Therefore, we can conclude that a lower pitch is more suitable for the hybridized configuration.

For the other short missions (from #06 to #11) the battery-only configuration is the best in terms of mass and volume, and the most suitable battery technology is the NMC, In these cases, the target values of mass and volume are easily satisfied. Mission #11 is the only short mission where the battery is sized according to the power requisite. Note that missions #11 and #12 differ not only for the cruise altitude (Table 3) but also for the duration of the climb and cruise phases. In particular, mission #12 has a shorter climb (thanks to the reduced cruise altitude) but a longer cruise (see Fig. 10). The longer cruise makes a small hybridization degree with an LFP battery preferable to an NMC battery-only configuration.

To better understand the results of Table 7, the effect of FC contribution, battery technology, onboard charging, and flight time will be discussed with particular reference to mission #02.

### 5.1. Increasing the fuel cell contribution (with onboard battery charge)

The plot of Fig. 15 shows the results of the application of the methodology for mission #02 when the fuel cell is allowed to charge the LFP battery. Similar results are obtained for the other long missions.

**Table 8**
Overall results of the parametric study (*min mass*) for the short missions.

| Mission | #06 | #07 | #08 | #09 | #10 | #11 | #12 |
|---|---|---|---|---|---|---|---|
| Battery type | NMC | NMC | NMC | NMC | NMC | NMC | LFP |
| Battery charge | N/A | N/A | N/A | N/A | N/A | N/A | no |
| $x_{FC}$ (%) | - | - | - | - | - | - | 3 |
| FC size (kW) | - | - | - | - | - | - | 6 |
| $H_2$ (kg) | - | - | - | - | - | - | 0.2 |
| Bat. (kWh) | 22.8 | 26.5 | 22.8 | 20.2 | 18.8 | 19.8 | 11.9 |
| Tank (L) | - | - | - | | - | - | 4.6 |
| Tot. Mass (kg) | 134.8 | 156.6 | 134.7 | 119.1 | 111.3 | 117.2 | 113.5 |
| Tot Vol. (L) | 61.8 | 71.8 | 61.7 | 54.6 | 51 | 53.7 | 68.5 |
| Sizing criterium. | $\Delta E_{batt}$ | $\Delta E_{batt}$ | $\Delta E_{batt}$ | $\Delta E_{batt}$ | $\Delta E_{batt}$ | $P_{batt}$ | $\Delta E_{batt}$ |

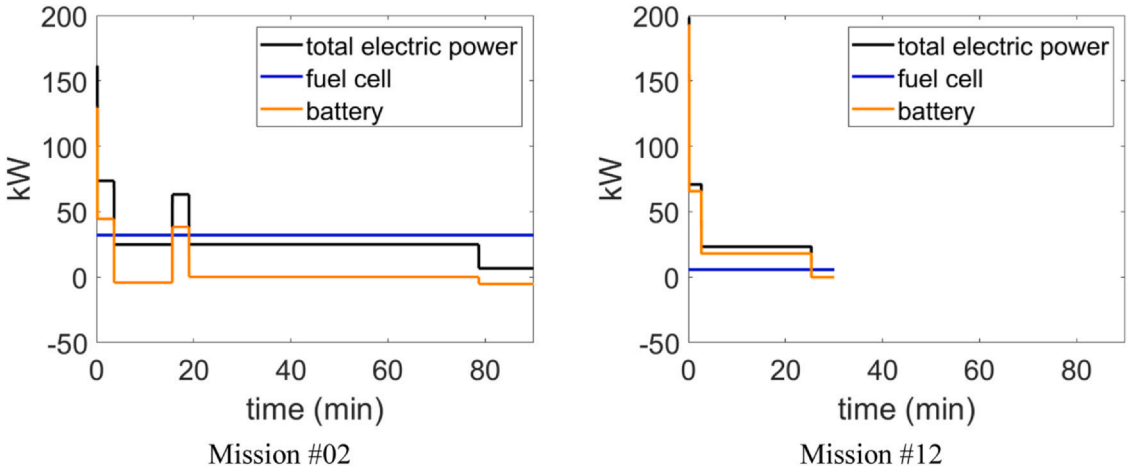


**Fig. 14.** Power distribution along the mission for the *min mass* configuration.

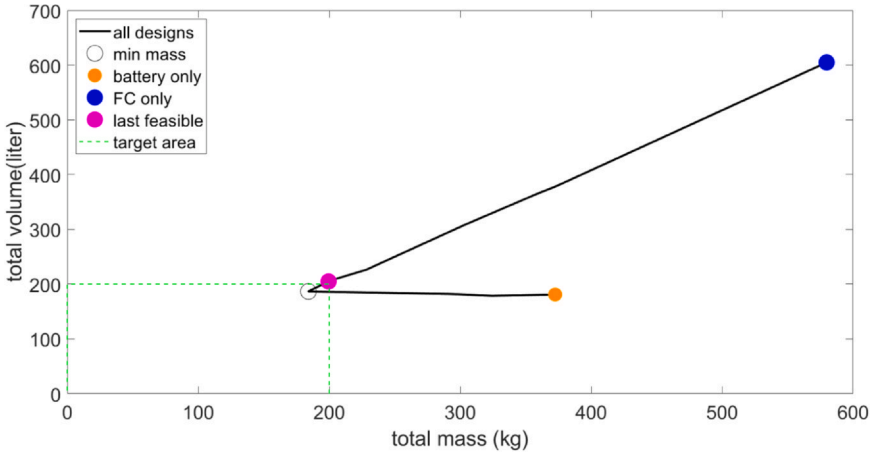


**Fig. 15.** Results of the methodology for mission #02 with battery charge.

The plot represents the globality of the designs considered in the investigation with $x_{FC}$ that increases from zero (orange bubble) to 100 (blue bubble). Starting from the bottom (battery only), the mass of the hybrid electric configuration initially decreases with $x_{FC}$ while the volume increases. This continues until reaching the optimum, "*min mass*", which corresponds to the lowest mass configuration compatible with the selected mission. This solution can be accepted if it falls within the target area outlined by the dotted green line. For mission #02, the *min mass* configuration allows a reduction of total weight by 50 % compared with the battery-only case while the occupied space is only 3 % higher. A further increase in $x_{FC}$ determines an increase in both mass and volume until reaching the *last feasible* solution that corresponds to a fully charged battery at the end of the mission.

Once the *last feasible* configuration is reached, a further increase in the fuel cell contribution, $x_{FC}$, corresponds to a battery that is partially discharged at the beginning of the mission and fully charged at the end. This means that a certain amount of the hydrogen energy is stored in electricity form during the flight. This kind of behavior is considered *unfeasible*. Using the definitions of Pornet et al (Pornet and Isikveren, 2015)., the minimum feasible hybridization degrees are 77.9 % in terms of power, Eqs. (2), and 11.4% in terms of energy, Eq. (3).

Discontinuities in the black line of Fig. 15 are due to transition from battery sized for energy and battery sized for power or to the saturation of the maximum charge current for the lower power phases (in the order descent, cruise1, cruise 2, climb2).

The details of the mass contributions are reported in Fig. 16 where the mass of battery, fuel cell, and tank vs $x_{FC}$ are plotted together with the target of 200 kg (green line). The mass of the fuel cell is the most relevant for $x_{FC} > 16.4$ % because of its limited power density, while the battery is the critical component for $x_{FC} < 16.4$ %.

Fig. 17 shows the consumption of the hydrogen and the final state of charge of the battery vs $x_{FC}$.

In the case of *min mass* configuration, the final state of charge is 32.8 % while in the *last feasible* configuration, the battery is fully charged at the end of the mission, and no external charge is required. This configuration requires a slightly higher volume and mass than the *min mass* configuration. To better understand what happens to the battery in the two cases, the trend of battery residual energy (state of the charge) for the three configurations (*battery only*, *min mass,* and *last feasible*) is compared in Fig. 18. In the *min mass* case, the battery is charged only during descent while in the last feasible configuration, the fuel cell produces more power than required for the cruise phases allowing battery charge even in cruise.

### 5.2. Increasing the fuel contribution (without on-board battery charge)

The results of the analysis without the option of charging the battery are shown in Fig. 19. The *min mass* configuration is the same as found in the previous cases in terms of fuel cell and battery, but the size of the hydrogen vessel is smaller because the battery is not charged. This determines a reduction of mass and volume compared with the previous case (*"with charge"*).

In this case, the *last feasible* solution corresponds to the battery being used at takeoff and climbs, while the rest of the mission is performed by using the fuel cell only. Fig. 20 shows that a further increase in the size

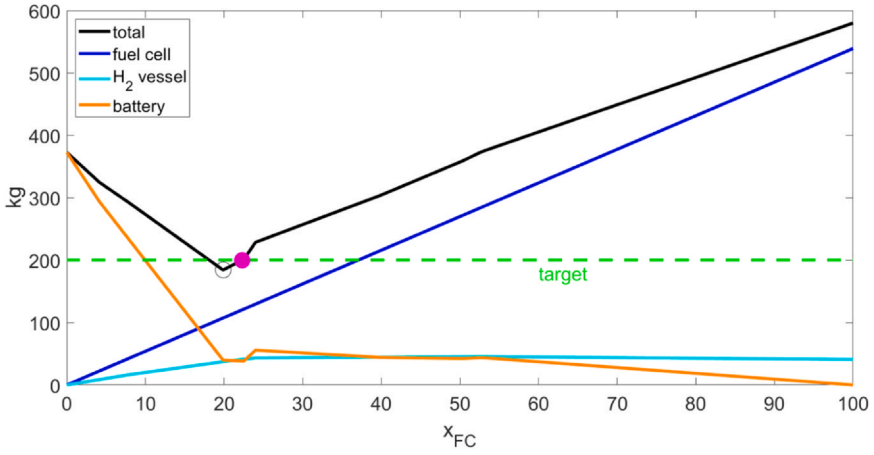


**Fig. 16.** Mass vs fuel cell contribution for mission #02 with battery charge.

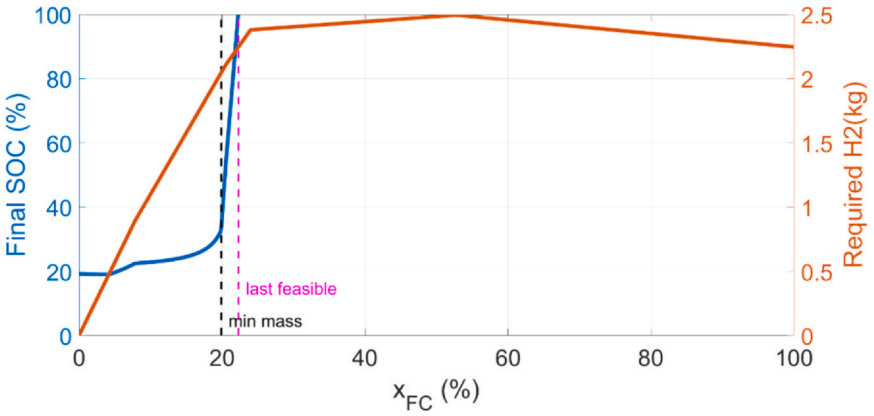


**Fig. 17.** Final SOC and required hydrogen for mission #02 with battery charge.

of the fuel cell beyond the value of $x_{FC}$ does not affect the results in terms of final SOC and required hydrogen (because of the negligible contribution of takeoff to the energy request) but determines only an increase of mass and volume of the fuel cell, with the battery becoming smaller and smaller. The trend of the state of charge for the *min mass*, *last feasible*, and *battery-only* configurations are compared in Fig. 21.

### 5.3. Charge depleting vs charge sustaining

It can be interesting to compare the *min mass* solution *w/o charge* with the *last feasible* case with charge. The first one corresponds to the minimum consumption of hydrogen (smaller $H_2$ vessel) but requires a full charge of the battery before the aircraft can fly again. In other words, this corresponds to a charge-depleting strategy (CD). Since the battery charge is a time-consuming process, this choice would strongly affect the availability of the aircraft. The second one, the *last feasible,* corresponds to a Charge Sustaining (CS) policy where battery charge between two consecutive flights is not required. The two configurations are compared in Table 9 for mission #02. The charge-sustaining configuration requires a larger fuel cell but needs a smaller battery.

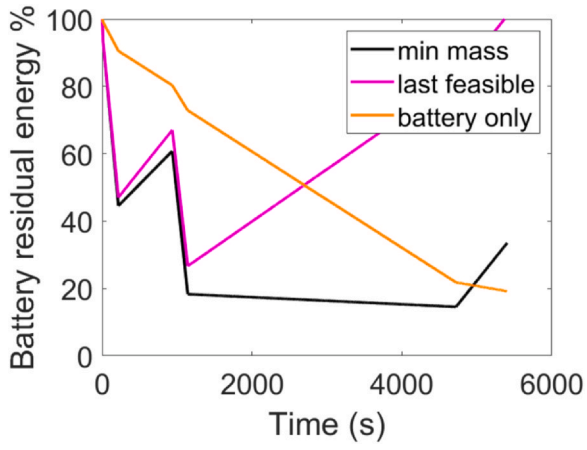


**Fig. 18.** Battery residual energy along mission #02 with charge.

The charge-depleting solution, compared with the CS one, allows a saving of hydrogen by 11 %. On the other hand, in the case of charge depletion, the battery will be fully discharged at the end of the mission, and additional time and energy will be needed to charge the battery before the next flight.

### 5.4. Battery technology

The plot of Fig. 22 shows the volume vs mass trends obtained with the five batteries in the case of no battery charge for mission #02. The size of the bubbles represents the fuel cell contribution $x_{FC}$.

The results of the methodology applied to all missions are reported in the Appendix in terms of mass vs volume trend for the five battery IDs. For missions #06-#11, as already discussed, the *min mass* configuration corresponds to a battery-only power system. Any value of $x_{FC}$ greater than 0 determines an increase in both weight and volume.

The analysis of the data of Fig. 22 and those reported in the Appendix reveals the NCA technology, despite having the highest values of VED and GED, performs poorly in all missions because of its limited $C_{rate,dis}$. In fact, the sizing criterion is always the power request for this battery. On the other hand, the NMC is the best technology in terms of

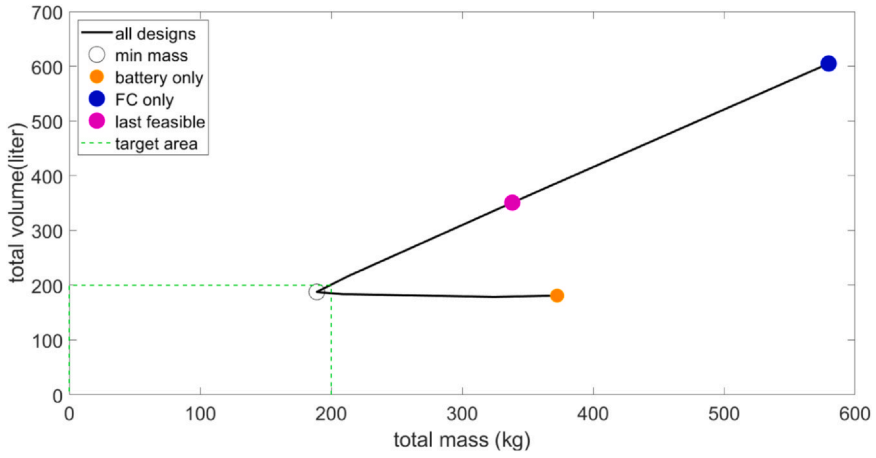


**Fig. 19.** Results of the methodology for long mission #02 w/o battery charge.

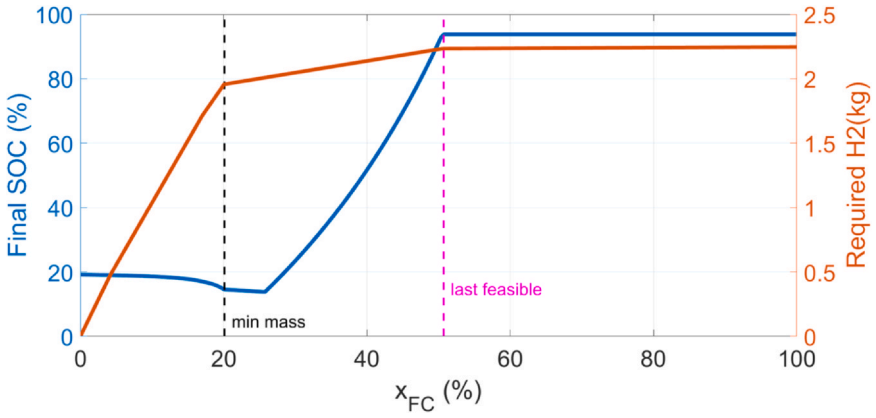


**Fig. 20.** Final SOC and required hydrogen for mission #02 without battery charge.

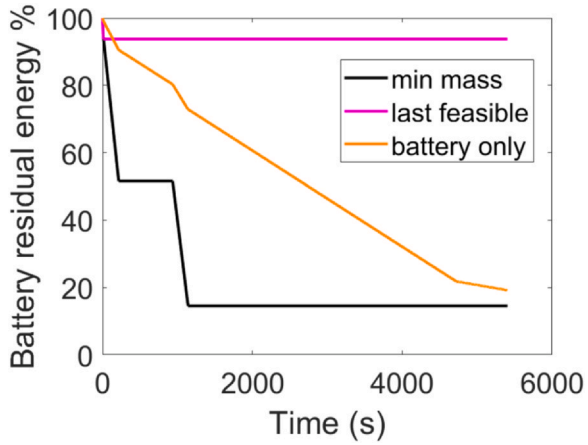


**Fig. 21.** Battery residual energy along the mission #02 w/o charge.

volume (thanks to the high values of VED), but the *min mass* configuration is obtained with LFP batteries being the power request the critical issue in the sizing process.

The CD and CS solutions obtained for mission #02 with the NMC battery are compared in Table 10 and Table 11 with the *min mass* configuration found by the sizing methodology for the choice of the final configuration.

### 5.5. Flight time

The application of the methodologies to missions #06 and #11 disclosed that a simple battery-only configuration is preferable when the flight time is 30 min. Using as reference mission #02, the role of flight time in defining the preference for the hybrid configuration with a fuel cell is addressed by changing the flight time of cruise2 so that the whole mission lasts from 20 to 120 min. The results are collected in Table 12.

For a flight time of up to 25 min, the optimal configuration is the battery-only. Increasing the flight time up to 30 min, the *min mass* configuration consists of a very small fuel cell equipped with a large battery. From 45 min upwards, the optimal size of the battery and the fuel cell remains almost constant, and the optimal configurations differ only for the size of the hydrogen storage system (since more hydrogen is needed to complete a longer mission).

**Table 9**
Charge Depleting vs Charge Sustaining (mission #02).

| mission | FC size (kW) | Battery size (kWh) | Consumed $H_2$ (kg) | Tank volume (L) | Total mass (kg) | Total volume (L) |
|---|---|---|---|---|---|---|
| CD (w/o on-board battery charge) | 32.5 | 5.9 | 1.96 | 57.4 | 189.0 | 187.6 |
| CS (full on-board charging) | 35.7 | 5.0 | 2.2 | 65.4 | 198.2 | 203 |

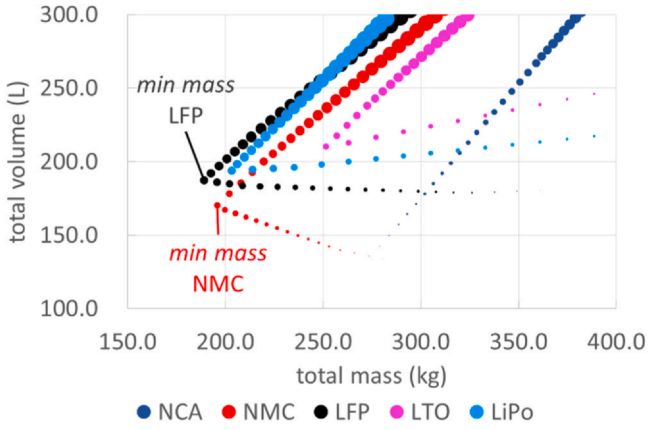


**Fig. 22.** Total volume vs total mass of the power system for mission #02 without on-board charge. The size of the bubbles represents the fuel cell contribution $x_{FC}$.

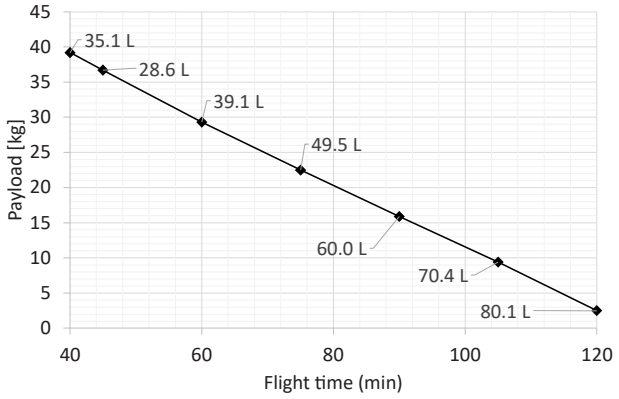


**Fig. 23.** Payload vs flight time according to the size of the hydrogen vessel.

Since the overall mass of the aircraft was kept constant in this investigation, the difference between the target mass of 200 kg and the optimal value of Table 12 can be translated into an additional payload. The plot of Fig. 23 shows the tradeoff between payload and flight time that can be obtained for mission #02 with a 5.2kWh LFP battery and a 32.2 kW fuel cell, by increasing the size of the hydrogen tank.

## 6. Economic and environmental issues

For a more complete analysis of the configurations reported in Table 10 and Table 11, the cost, safety, and environmental impact of these configurations is here addressed.

An NMC battery is about 30 % more expensive than an LFP one (ANON, 2023i). According to (ANON, 2023j) the cost per stored energy of LFP and NMC is 70.0 €/kWh and €100.0 €/kWh, respectively. Finding information about the cost per kW of fuel cell in the range of power 20–40 kW is not easy to find. Personal communication with a manufacturer revealed a cost of about 3000 €/kW for the stack. However, since most of the cost of the fuel cell is associated with its balance of plant and its control, the overall cost of the fuel system should be less affected by the fuel cell size. The cost of the pressurized hydrogen tank can be assumed equal to €700 per kg of hydrogen, according to Shin et al (Shin and Ha, 2023). The cost of refilling the hydrogen tank and charging the battery is assumed negligible.

Using the unit costs reported above for each component, the overall cost of the four alternatives can be estimated in Table 13. The minimum cost of the fuel cell in the proposed propulsive system is obtained with an NMC battery and a CD strategy. The choice of a CD configuration is in line with similar works in the scientific literature ( (Lapeña-Rey et al., 2007; Miazga et al., 2021).

However, the higher thermal runaway temperature (see Table 1) makes the LFP technology the preferred option for the retrofitting of the Seagull aircraft, especially in the case of CS strategy since the cost of the two alternatives is quite the same.

**Table 10**
Charge Depleting optimal configuration with batteries LFP and NMC (mission #02).

| mission | FC size (kW) | Battery size (kWh) | Consumed $H_2$ (kg) | Tank volume (L) | Total mass (kg) | Total volume (L) |
|---|---|---|---|---|---|---|
| CD (LFP) | 32.5 | 5.9 | 1.96 | 57.4 | 189.0 | 187.6 |
| CD (NMC) | 25.5 | 13.6 | 1.61 | 47.1 | 195.5 | 169.2 |

**Table 11**
Charge Sustaining optimal configuration with batteries LFP and NMC (mission #02).

| mission | FC size (kW) | Battery size (kWh) | Consumed $H_2$ (kg) | Tank volume (L) | Total mass (kg) | Total volume (L) |
|---|---|---|---|---|---|---|
| CS (LFP) | 35.7 | 5.0 | 2.2 | 65.4 | 198.2 | 203 |
| CS (NMC) | 33.5 | 12.8 | 2.1 | 64.7 | 227.5 | 211 |

**Table 12**
Effect of total flight time (LFP battery, no-charge, mission #02).

| Total time (min) | FC size (kW) | Battery size (kWh) | Consumed $H_2$ (kg) | Tank volume (L) | Total mass (kg) | Total volume (L) |
|---|---|---|---|---|---|---|
| 20 | 0 | 16.0 | 0 | 0 | 122.5 | 59.5 |
| 25 | 0 | 16.0 | 0 | 0 | 122.5 | 59.5 |
| 30 | 6.1 | 13.9 | 0.17 | 4.8 | 129.8 | 76.8 |
| 40 | 31.5 | 5.24 | 0.85 | 35.1 | 160.8 | 149.7 |
| 45 | 31.7 | 5.3 | 0.97 | 28.6 | 163.3 | 153.6 |
| 60 | 32.0 | 5.20 | 1.33 | 39.1 | 170.7 | 165.1 |
| 75 | 32.0 | 5.24 | 1.67 | 49.5 | 177.5 | 175.6 |
| 90 | 32.2 | 5.18 | 2.05 | 60.0 | 184.1 | 186.5 |
| 105 | 32.2 | 5.19 | 2.4 | 70.4 | 190.6 | 197.0 |
| 120 | 32.2 | 5.25 | 2.75 | 80.1 | 197.5 | 207.6 |

**Table 13**
Estimated costs of the proposed alternatives.

| | battery | fuel cell | tank | total |
|---|---|---|---|---|
| CD (LFP) | 413.00 € | 97,500.00 € | 1372.00 € | 97,913.00 € |
| CD (NMC) | 1360.00 € | 76,500.00 € | 1127.00 € | 77,860.00 € |
| CS (LFP) | 350.00 € | 107,100.00 € | 1540.00 € | 107,450.00 € |
| CS (NMC) | 1280.00 € | 100,500.00 € | 1470.00 € | 101,780.00 € |

Regarding the environmental impact, all the power systems analyzed here are "zero-emission" only if one limits the analysis to the direct emissions produced during the usage and neglects the environmental impact of the water generated by the chemical reaction taking place in the fuel cell. The indirect environmental impact of the proposed power systems, on the contrary, depends on the emission intensity of the electricity generation system (only for the CS configurations) and the hydrogen production process (Donateo and Çinar, 2022). The comparison in terms of life cycle assessment (LCA) is too complex to be performed here because it requires a full analysis of the energy consumption and environmental impact related to the raw material extractions, manufacturing and processing, transportation, usage, and waste disposal of all components.

## 7. Limits of this investigation and future studies

The proposed methodology is based on a very simple modeling approach, in particular for the fuel cell. In fact, the net efficiency of the fuel cell stack is assumed constant, independently of load and altitude and the design of the balance of plant is integrated with the fuel cell stack. This choice was due to the lack of information on the actual BOP adopted in commercially available fuel cells, that will be used to obtain a mock-up of the hybrid electric power system. To this scope, a modular configuration will be considered. This choice is motivated by the need to ensure sufficient remaining power in case of failure of one or two stacks. Moreover, the use of a modular configuration allows the deactivation of one or more stacks during the low-power phases of the flight. The mock-up will be assembled and tested at the laboratories of the Department of Engineering for Innovation at the University of Salento using two bidirectional power supplies (Tian et al., 2024) and real time simulators to verify the behavior of the whole system (fuel cell and battery) under realistic operating conditions (see (Donateo and Totaro, 2018) and compare passive and active configurations.

In addition to the simplifications in the analysis of the losses in fuel cells, electric motors, electronics, etc., another limit of the proposed modelling approach is and the lack of a dynamic analysis of the system. These limitations will be overcome in next future by proposing a dynamic model of the powertrain and more realistic missions to be validated on the mock-up.

## 8. Conclusions

The sizing of a hybrid electric propulsive system with a fuel cell for ultralight aircraft was performed in this investigation using a simple methodology that minimizes the mass of the power system at constant take-off weight while complying with space constraints and technological limits of batteries. Twelve different missions were considered, performed with a rule-based energy management strategy compatible with a passive hybrid electric configuration. The fuel cell power working point was kept constant along the mission when compatible with the battery technological limits in terms of charge and discharge. The procedure, although being much simpler than other methods proposed for fuel cell power system in automotive applications, is suitable for the aerospace application where most of the time (cruise) the vehicle requires a constant power.

The procedure was applied to the retrofitting of ultralight aircraft with on-the-market products for batteries, fuel cells, and hydrogen vessels. The procedure allowed the identification of the most suitable type of lithium batteries (among the five technologies included in the analysis) and the optimal size of the fuel cell, battery, and pressurized hydrogen tank.

The analysis of different missions that differ for cruise speed, propeller pitch setting, altitude, climb rate, and duration of the flight segments, together with careful consideration of the technological limits of commercial technologies, allowed us to reach the following general conclusions.

- Despite having the highest values of energy density, NCA batteries perform poorly in hybrid electric configurations because of their limited power density. Li-po batteries, on the other hand, present the highest values of power density but are penalized by their low energy density. NMC and LFP presents an interesting trade-off between power and energy per unit of mass.
- For missions below 30 min of flight time, it is better to employ a simple electric power system with an NMC battery as the only energy source.
- Given the same duration of the mission, the advantage of using a fuel cell depends on the cruise time and altitude.
- For the long missions (90 min), the adoption of a hybrid electric power system determines a reduction of the weight. The best results in terms of mass are obtained with LFP batteries that present a higher power density than NCAs and NMCs. Moreover, they are also safer thanks to their higher thermal runaway temperature.
- The optimal size of the fuel cell does not coincide with the cruise power of the mission because of the reduction of fuel cell power with altitude caused by the higher parasitic power of the compressor.
- The space occupied by the fuel cell was found to be a critical issue, and the target of an overall volume below 200 L difficult to meet with the desired flight time of 90 min. The NMC batteries are a good choice to minimize the occupied space and to reduce the costs of the overall power system.
- The volume and mass of the hydrogen vessel increase linearly with cruise flight time while the optimal size of the battery and fuel cell is almost the same between 45 and 120 min.
- Because of the limited charging rate of NMC and LFP batteries, using the fuel cell to charge the battery onboard does not change the optimal size of the fuel cell and the battery, but determines an increase in the total mass because of the higher hydrogen consumption.
- As a safeguard from the degradation in the propeller efficiency, the battery can be oversized while the fuel cell size and the hydrogen storage can remain the same.
- A lower pitch setting for the propeller was found to be more suitable for the hybridized configuration.
- Future studies are needed to verify the behaviour of the hybrid electric power system under transient conditions of load and altitude.

## CRediT authorship contribution statement

**Teresa Donateo:** Writing – review & editing, Writing – original draft, Supervision, Data curation, Conceptualization. **Antonio Ficarella:** Funding acquisition, Project administration. **Leonardo Lecce:** Data curation, Resources.

## Data availability

Data will be made available on request.

## Declaration of Competing Interest

The authors declare that they have no known competing financial interests or personal relationships that could have appeared to influence the work reported in this paper.

## Acknowledgment

This investigation is part of the project "Sviluppo di architetture propulsive ad emissioni zero per l'Aviazione generale (SERENA - CUP: F89J22003510004)", funded by the Italian Ministry for the Environment and Energy Security (MASE), M2-C2-I3.5 call of the Italian Recovery and Resilience Plan. The authors wish to thank the other partners of the project (DTA-Scarl and EngineSoft s.p.a.) for their valuable suggestions and helpful support.

## Appendix

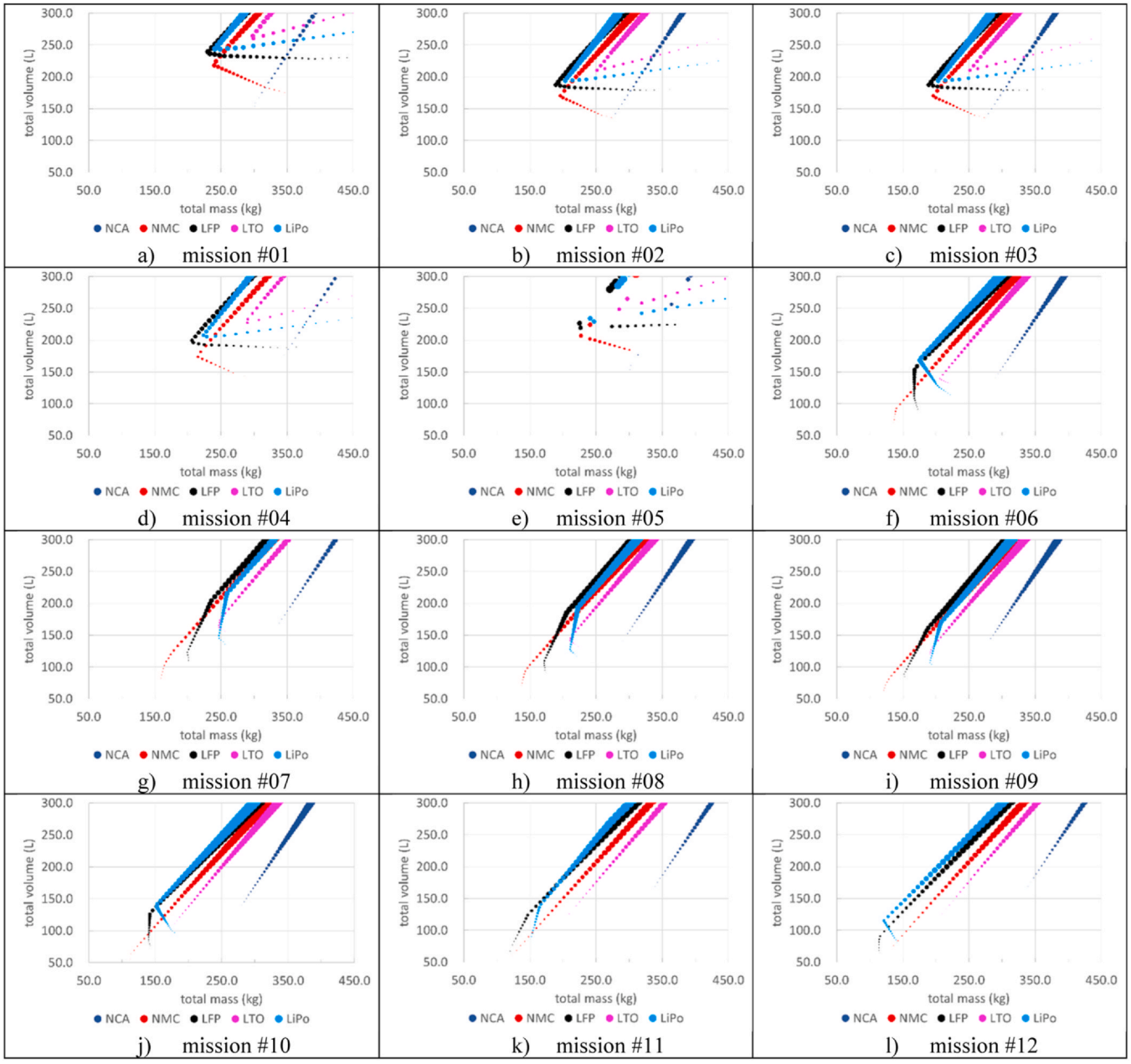


**Fig. 24.** Results of the sizing procedure without battery charge. The size of the bubble represents the fuel cell contribution $x_{FC}$.

## References


ANON ⟨https://www.capacitorsite.com/lithium.html⟩, retrieved on 26 october 2023b.

ANON ⟨https://www.hydrogenfuelnews.com/hyflyer-i-ii-hydrogen-aircraft/8551943/⟩ (accessed on October 2023g).

ANON ⟨https://ec.europa.eu/commission/presscorner/detail/en/MEMO_16_2497⟩ (retrieved on 1 September 2023a).

ANON ⟨https://www.flashbattery.tech/en/types-of-lithium-batteries-which-chemistry-use/⟩ retrieved on 26 october 2023c.

ANON ⟨https://www.airenergy.de/en/⟩, retrieved on 26 october 2023f.

ANON ⟨https://www.horizoneducational.com/120kw-liquid-cooled-hydrogen-fuel-cell-vl-series/p1574⟩, Retrieved on 2 September, 2023h.

ANON ⟨https://www.ecolithiumbattery.com/lfp-vs-nmc-battery/⟩ retrieved on 22 november 2023i.

ANON ⟨https://batteryuniversity.com/article/bu-205-types-of-lithium-ion⟩, retrieved on 26 october 2023d.

ANON ⟨https://www.pdbattery.com/rc-aircraft-battery.html⟩, retrieved on 26 october 2023e.

ANON ⟨https://www.eetimes.com/lithium-batteries-for-evs-go-nmc-or-lfp/⟩, retrieved on 22 november 2023j.

Arista A., Ferraro M., Sergi F., Antonucci V. Dynamic Model of High-Performance Li-ion cells (LiFePO4, Li-Polymers and LiFP6 NBC) in different load conditions, *Proceedings of the 6th IC-EpsMsO*, Athens, Greece, 8–11 July 2015.

Ayar, M., Karakoc, T.H., 2023. Decision mechanism between fuel cell types: a case study for small aircraft. Int. J. Hydrog. Energy, vol 48, 23156–23167.

Barroso, J., Renau, J., Lozano, A., Miralles, J., Martin, J., Sanchez, F., Barreras, F., 2015. Experimental determination of the heat transfer coefficient for the optimal design of the cooling system of a PEM fuel cell placed inside the fuselage of an UAV. Appl. Therm. Eng. 89, 1–10.

Beyers, I., Bensmann, A., Hanke-Rauschenbach, R., 2023. Ragone plots revisited: a review of methodology and application across energy storage technologies. J. Energy Storage 73, 109097.

Boukoberine, M.N., Zia, M.F., Benbouzid, M., Zhou, Z., Donateo, T., Hybrid fuel cell powered drones energy management strategy improvement and hydrogen saving using real flight test data,

Bradley, T.H., Moffitt, B.A., Mavris, D.N., Parekh, D.E., 2007. Development and experimental characterization of a fuel cell powered aircraft. J. Power Sources Volume 171 (Issue 2), 793–801. https://doi.org/10.1016/j.jpowsour.2007.06.215

Camargos, P.H., dos Santos, P.H., dos Santos, I.R., Ribeiro, G.S., Caetano, R.E., 2022. Perspectives on Li-ion battery categories for electric vehicle applications: a review of state of the art. Int. J. Energy Res. 46 (13), 19258–19268.

Chen, F., Yu, Y., Gao, Y., 2017. Temperature control for proton exchange membrane fuel cell based on current constraint with consideration of limited cooling capacity. Fuel Cells 17 (No. 5), 662–670.

Datta A., PEM Fuel Cell MODEL for Conceputal Design of Hydrogen eVTOL Aircraft, Nasa Report, 2021, 20210000284.

Donateo, T., 2023. Semi-empirical models for stack and balance of plant in closed-cathode fuel cell systems for aviation. Energies 16 (22), 7676.

Donateo, T., Çinar, H., 2022. Conceptual design and sizing optimization based on minimum energy consumption of lift-cruise type eVTOL aircraft powered by battery and fuel cell for urban air mobility. J. Phys.: Conf. Ser. Vol. 2385 (No. 1), 012072.

Donateo, T., Spedicato, L., 2017. Fuel economy of hybrid electric flight. Appl. Energy 206, 723–738.

Donateo, T., Totaro, R., 2018. Hybridization of training aircraft with real world flight profiles. Aircr. Eng. Aerosp. Technol. 91 (2), 353–365.

Gao, Y., Jausseme, C., Huang, Z., Yang, T., 2022. Hydrogen-powered aircraft: hydrogen–electric hybrid propulsion for aviation. IEEE Electrification Mag. 10 (2), 17–26.

Geliev, A.V., Varyukhin, A.N., Zakharchenko, V.S., Kiselev, I.O., Zhuravlev, D.I., 2019. Conceptual design of an electric propulsion system based on fuel cells for an ultralight manned aircraft. 21-25 Oct.. 2019 Int. Conf. Electrotech. Complex. Syst. (ICOECS), Ufa, Russ. 1–17.

Gong, C., Xing, L., Liang, C., Tu, Z., 2022. Modeling and dynamic characteristic simulation of air-cooled proton exchange membrane fuel cell stack for unmanned aerial vehicle. Renew. Energy 188, 1094–1104.

Jarry, T., Lacressonnière, F., Jaafar, A., Turpin, C., Scohy, M., 2021a. Modeling and sizing of a fuel cell—lithium-ion battery direct hybridization system for aeronautical application. Energies 14 (22), 7655.

Jarry, T., Lacressonnière, F., Jaafar, A., Turpin, C., Scohy, M., 2021b. Optimal sizing of a passive hybridization fuel cell–battery. 09-10 December. 2021 Int. Conf. Electr., Comput. Energy Technol. (ICECET) Cape Town - South Afr. 1–6.

Kabalo, M., Blunier, B., Bouquain, D., Miraoui, A., 2010. State-of-the-art of DC-DC converters for fuel cell vehicles. Lille, France, 1– 3 Sept.. 2010 IEEE Veh. Power Propuls. Conf. 1–6.

Kasim, A.A., Marek, E.J., 2022. Performance and failure analysis of a retrofitted cessna aircraft with a fuel cell power system fuelled with liquid hydrogen. J. Power Sources 521, 230987.

Kim, T., Kwon, S., 2012. Design and development of a fuel cell-powered small, unmanned aircraft. Int. J. Hydrog. Energy 37 (1), 615–622.

Lapeña-Rey, N., Mosquera, J., Bataller, E., Ortí, F., The boeing fuel cell demonstrator airplane *SAE Technical Paper*, 2007, No. 2007–01-3906.

Liu, H., Yao, Y., Wang, J., Qin, Y., Li, T., 2022. A control architecture to coordinate energy management with trajectory tracking control for fuel cell/battery hybrid unmanned aerial vehicles. Int. J. Hydrog. Energy 47 (34), 15236–15253.

Lü, X., Wu, Y., Lian, J., Zhang, Y., Chen, C., Wang, P., Meng, L., 2020. Energy management of hybrid electric vehicles: a review of energy optimization of fuel cell hybrid power system based on genetic algorithm. Energy Convers. Manag. 205, 112474.

Marksel, M., Prapotnik Brdnik, A., 2022. Maximum take-off mass estimation of a 19-seat fuel cell aircraft consuming liquid hydrogen. Sustainability 14 (14), 8392.

Mazzeo, F., Di Ilio, G., 2024. Fuel cell hybrid electric propulsion system for a lightweight helicopter: design and performance analysis in urban air mobility scenario. Int. J. Hydrog. Energy Volume 50 (Part B), 891–907.

McCormick, B.W., 1995. Aerodynamics, aeronautics and flight mechanics. John Wiley, New York, USA.

Mercier, V., Ceschia, A., Azib, T., Larouci, C., 2023. Pre-Sizing approach of a fuel cell-battery hybrid power system with interleaved converters. Energies 16 (10), 4068.

Miazga, T., Iwański, G., Nikoniuk, M., 2021. Energy conversion system and control of fuel-cell and battery-based hybrid drive for light aircraft. Energies 14 (4), 1073.

Moffitt, B., Bradley, T., Mavris, D., Parekh, D., 2006. Design space exploration of small-scale PEM fuel cell long endurance aircraft (September). 6th AIAA Aviat. Technol., Integr. Oper. Conf. (ATIO) Wichita, Kans. 25 - 27, 7701.

Motapon, S.N., Dessaint, L.A., Al-Haddad, K., 2013. A comparative study of energy management schemes for a fuel-cell hybrid emergency power system of more-electric aircraft. IEEE Trans. Ind. Electron. 61 (3), 1320–1334.

Nexa Power Module User's Manual, Ballard Power Systems User Manual MAN51 00.

Nicolay, S., Karpuk, S., Liu, Y., Elham, A., 2021. Conceptual design and optimization of a general aviation aircraft with fuel cells and hydrogen. Int. J. Hydrog. Energy 46 (64), 32676–32694.

Nishizawa, A., Kallo, J., Garrot, O., Weiss-Ungethüm, J., 2013. Fuel cell and Li-ion battery direct hybridization system for aircraft applications. J. Power Sources 222, 294–300.

Onori, S., Serrao, L., Rizzoni, G., 2016. Hybrid electric vehicles: Energy management strategies. Springer, London.

Papadopoulos, E., Aggelakakis, A., Tromaras, A., 2018. The future of the european transport sector: identifying the key trends regarding the transport concepts of the future (September). Int. Conf. Traffic Transp. Eng. – ICTTE, Belgrade, Serb.

Park, J., Lee, D., Yee, K., 2022a. Development of fuel cell/battery hybrid system sizing methodology for eVTOL aircraft. Chicago, Illinois and Online, 27 June - 1 July. AIAA Aviat. 2022 Forum 2022 3514.

Park, J., Lee, D., Lim, D., Yee, K., 2022b. A refined sizing method of fuel cell-battery hybrid system for eVTOL aircraft. Appl. Energy 328, 120160.

Pisapia, A.M., Volza, A., Savioli, T., Martini, P., Mattarelli, E., 2023. Hybrid-electric power unit for an ultralight aircraft. J. Phys.: Conf. Ser. Vol. 2648 (No. 1), 012081.

Pornet, C., Isikveren, A.T., 2015. Conceptual design of hybrid-electric transport aircraft. Prog. Aerosp. Sci. 79, 114–135.

Pratt, J.W., Brouwer, J., Samuelsen, G.S., 2007. Performance of proton exchange membrane fuel cell at high-altitude conditions. J. Propuls. Power 23 (2), 437–444.

Rathke, P., Thalau, O., Kallo, J., Schirmer, J., Stephan, T., 2014. Long distance flight testing with the fuel cell powered aircraft Antares DLR-H2. Dtsch. Ges. für Luft. -und Raumfahrt-Lilienthal-Obert-.-. eV.

Romeo, G., Cestino, E., Correa, G., Borello, F., 2011. A fuel cell based propulsion system for general aviation aircraft: the ENFICA-FC experience. SAE Int. J. Aerosp. 4, 724–737 (2011-01-2522).

Rubio, F., Llopis-Albert, C., Besa, A.J., 2023. Optimal allocation of energy sources in hydrogen production for sustainable deployment of electric vehicles. Technol. Forecast. Soc. Change 188, 122290.

Shin, H.K., Ha, S.K., 2023. A review on the cost analysis of hydrogen gas storage tanks for fuel cell vehicles. Energies 16 (13), 5233.

Song, W.J., Chen, H., Guo, H., Ye, F., Li, J.R., 2022. Research progress of proton exchange membrane fuel cells utilizing in high altitude environments. Int. J. Hydrog. Energy 47.

Sparano, M., Sorrentino, M., Troiano, G., Cerino, G., Piscopo, G., Basaglia, M., Pianese, C., 2023. The future technological potential of hydrogen fuel cell systems for aviation and preliminary co-design of a hybrid regional aircraft powertrain through a mathematical tool. Energy Convers. Manag. 281, 116822.

Suewatanakul, S., Porcarelli, A., Olsson, A., Grimler, H., Chiche, A., Mariani, R., Lindbergh, G., 2022. Conceptual design of a hybrid hydrogen fuel cell/battery blended-wing-body unmanned aerial vehicle—an overview. Aerospace 9 (5), 275.

Taccani, R., Malabotti, S., Dall'Armi, C., Micheli, D., 2020. High energy density storage of gaseous marine fuels: an innovative concept and its application to a hydrogen powered ferry. Int. Shipbuild. Prog. 67 (1), 33–56.

Thomas, C.E., 2009. Fuel cell and battery electric vehicles compared. Int. J. Hydrog. Energy 34 (15), 6005–6020.

Tian, W., Liu, L., Zhang, X., Shao, J., Ge, J., 2024. Adaptive hierarchical energy management strategy for fuel cell/battery hybrid electric UAVs. Aerosp. Sci. Technol. 146, 108938.

Tolj, I., Penga, Ž., Vukičević, D., Barbir, F., 2020. Thermal management of edge-cooled 1 kW portable proton exchange membrane fuel cell stack. Appl. Energy 257, 114038.

WAN, W.M., 2015. Cooling channels design analysis with chaotic laminar trajectory for closed cathode air-cooled PEM fuel cells using non-reacting numerical approach. IOP Conf. Ser.: Mater. Sci. Eng. Vol. 88 (No. 1), 012065.

Wang, C., Amietszajew, T., Carvajal, R., Guo, Y., Ahmed, Z., Zhang, C., Bhagat, R., 2021a. Cold ageing of nmc811 lithium-ion batteries. Energies 14 (16), 4724.

Wang, Y.-X., Chen, Q., Zhang, J., He, H., 2021b. Real-time power optimization for an air-coolant proton exchange membrane fuel cell based on active temperature control. Energy 220, 119497.

Wright, S., Aaltonen, J., 2022. Fuel cells and novel thermal management advancements required for aviation (September). 33rd Congr. Int. Counc. Aeronaut. Sci. ICAS2022, Stockh. Swed. 4–9 (September).

Wróblewski, P., 2022. Analysis of torque waveforms in two-cylinder engines for ultralight aircraft propulsion operating on 0W-8 and 0W-16 oils at high thermal loads using the diamond-like carbon composite coating. SAE Int. J. Engines 15 (1), 129–146.

Wróblewski, P., Świątek, P., Kachel, S., Zyska, T., 2023. Development and research of a hybrid power unit for ultralight aircraft: an innovative approach to energy efficiency and operational flexibility. Combust. Engines. https://doi.org/10.19206/CE174721

Xing, S., Zhao, C., Zou, J., Zaman, S., Yu, Y., Gong, H., Wang, H., 2022. Recent advances in heat and water management of forced-convection open-cathode proton exchange membrane fuel cells. Renew. Sustain. Energy Rev. 165, 112558.

Zhang, J., Xie, Z., Zhang, J., Tang, Y., Song, C., Navessin, T., et al., 2006. High temperature PEM fuel cells. J. Power Sour. 160 (2), 872–891.